# Effect of Acid Sphingomyelinase Deficiency in Type A Niemann-Pick Disease on the Transport of Therapeutic Nanocarriers Across the Blood-Brain Barrier

**Maximilian Loeck[1], Marina Placci[1], and Silvia Muro[1,2]**

[1]Institute for Bioengineering of Catalonia (IBEC) of the Barcelona Institute of Science and Technology, Barcelona, Spain

[2]Institution of Catalonia for Research and Advanced Studies (ICREA), Barcelona, Spain

*** Correspondence:** Silvia Muro; smuro@ibecbarcelona.eu

**Word count: 6978**

**ABSTRACT**

ASM deficiency in Niemann-Pick disease type A results in aberrant cellular accumulation of sphingomyelin, neuroinflammation, neurodegeneration, and early death. There is no available treatment because enzyme replacement therapy cannot surmount the blood-brain barrier (BBB). Nanocarriers (NCs) targeted across the BBB *via* transcytosis might help; yet, whether ASM deficiency alters transcytosis remains poorly characterized. We investigated this using model NCs targeted to intracellular adhesion molecule-1 (ICAM-1), transferrin receptor (TfR), or plasmalemma vesicle-associated protein-1 (PV1) in ASM-normal *vs*. ASM-deficient BBB models. Disease differentially changed the expression of all three targets, with ICAM-1 becoming the highest. Apical binding and uptake of anti-TfR NCs and anti-PV1 NCs were unaffected by disease, while anti-ICAM-1 NCs had increased apical binding and decreased uptake rate, resulting in unchanged intracellular NCs. Additionally, anti-ICAM-1 NCs underwent basolateral re-uptake after transcytosis, whose rate was decreased by disease, as for apical uptake. Consequently, disease increased the effective transcytosis rate for anti-ICAM-1 NCs. Increased transcytosis was also observed for anti-PV1 NCs, while anti-TfR NCs remained unaffected. A fraction of each formulation trafficked to endothelial lysosomes. This was decreased in disease for anti-ICAM-1 NCs and anti-PV1 NCs, agreeing with opposite transcytosis changes, while it increased for anti-TfR NCs. Overall, these variations in receptor expression and NC transport resulted in anti-ICAM-1 NCs displaying the highest absolute transcytosis in the disease condition. Furthermore, these results revealed that ASM deficiency can differently alter these processes depending on the particular target, for which this type of study is key to guide the design of therapeutic NCs.

**Keywords:** drug nanocarriers, blood-brain barrier, receptor-mediated transcytosis, ICAM-1, transferrin receptor, PV-1, lysosomal storage disease, ASM deficiency, Niemann-Pick disease type A.

**Graphical abstract:**

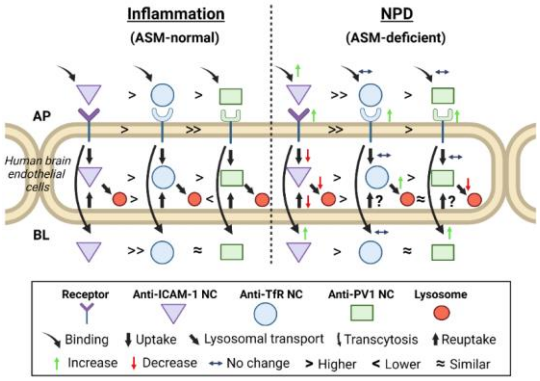

## 1 INTRODUCTION

Acid sphingomyelinase (ASM) deficiency, historically called Niemann-Pick disease types A or B, (NPD, OMIM #257200, #607616)[1,2], is a rare genetic disease belonging to the lysosomal storage disorders (LSDs) group, which results in aberrant accumulation of undegraded sphingomyelin in lysosomes within cells[3,4]. ASM is a lysosomal enzyme that cleaves sphingomyelin, a major component of cell membranes[5] and, therefore, crucial for maintaining sphingolipid homeostasis and participating in membrane turnover[6,7]. NPD type B is a debilitating disease affecting visceral organs such as liver, lungs, and spleen[8–10], whereas NPD type A (herein called NPD for simplicity) additionally affects the central nervous system (CNS), leading to rapid neurodegeneration and early mortality before the third year of life[11–14]. Both visceral and neurological manifestations associate with inflammation[4].

Olipudase Alpha, commercialized as Xenpozyme® by Sanofi, is a recombinant ASM product administered by intravenous (*i.v.*) infusion and used for enzyme replacement therapy (ERT), recently approved in Japan, Europe, and the US[15]. As most other lysosomal enzymes, Olipudase Alpha contains mannose-6-phophate (M6P) groups and, thus, can enter cells *via* clathrin-mediated endocytosis upon binding to the M6P receptor (M6PR) expressed on most cells of the body[16]. This drug is indicated for visceral forms of the disease where it has demonstrated therapeutic effects[15,17]. However, as most other protein therapeutics, this pharmaceutical cannot cross the blood-brain barrier (BBB) and, therefore, cannot be used to treat neuronopathic symptoms[18,19].

Nanomedicine, using nano-sized drug delivery systems called nanocarriers (NCs), offers an interesting platform to surmount this obstacle[18]. Different NCs have been investigated in the context of lysosomal ERTs, mostly lipid- and polymer-based nanoparticles, as well as extracellular vesicles[20–23]. Particularly regarding brain delivery of lysosomal ERTs, NC strategies have involved surface-functionalized lipid-core nanocapsules, surfactant-coated biodegradable nanoparticles, polymersomes, and poly(lactic-co-glycolide acid) (PLGA) nanoparticles[24–31]. Out of these studies, it was observed that formulations not targeted to endothelial markers associated with transcytosis did not improve brain delivery of lysosomal ERTs in animal models[24,25], while those targeted to transcytosis pathways did[26–31].

Specifically, formulations resulting in brain delivery of recombinant lysosomal enzymes were those targeting intracellular adhesion molecule 1 (ICAM-1), low-density lipoprotein receptor-related protein 1 (LRP-1), transferrin receptor (TfR), or opioid receptors[26–31]. ICAM-1 is a transmembrane glycoprotein overexpressed in pathologies associated with inflammation, including NPD, which associates with the cell adhesion molecule (CAM)-mediated pathway, a clathrin- and caveolae-independent route[32,33]. ICAM-1 targeted NCs have been shown to improve delivery of ASM, as well as other lysosomal enzymes, in cell cultures and *in vivo*[30,31,34–40]. CAM-mediated transcytosis from the apical side (AP; circulation side) to the basolateral side (BL; tissue side) of the endothelium, including the BBB, has been described both in cellular[30,41] and animal models after *i.v.* injection of ICAM-1-targeting NCs[30,31,36], with intra-arterial administration further increasing brain delivery[42]. Secondary brain targeting can occur when brain inflammation causes anti-ICAM-1 NCs from the lungs to be mobilized into the brain by leukocytes[43]. Regarding TfR, this marker associates with the clathrin-mediated pathway and has long been studied in the context of trans-BBB drug delivery[44–46]. LRP-1 has

been shown to relate to clathrin-coated pits and also lipid rafts[47,48], more classically relevant for caveolae-mediated pathways[49], and the mechanism mediating transport of NCs targeted to opioid receptors via the g7 glycopeptide is not fully characterized[50]. Instead, a well-established caveolar marker is plasmalemma vesicle-associated protein-1 (PV1), also known as Plvap, a protein that resides at the neck of caveoli and has been used to target NCs to endothelial cells (ECs)[51,52].

Despite these advances, there is a substantial lack of studies to comparatively examine these trans-BBB routes and whether LSDs, particularly ASM-deficiency in NPD, may alter their activity. This is plausible because a primary consequence of this disease is sphingomyelin accumulation in lysosomes and other cellular membranes[53,54]. Additionally, secondary accumulation of other lipids, such as cholesterol, lyso-sphingomyelin, glycolipids, and gangliosides, has been observed in NPD[53,55,56]. This lipid disbalance causes various pathological manifestations at the cellular level due to their key role on normal cell function, including alterations in processes related to membrane trafficking[57–61]. For instance, some cellular models and primary cells derived from patients have shown alterations in endocytosis of lipid and protein markers *via* clathrin-coated pits, caveoli, and macropinocytosis[62–65].

Therefore, to evaluate this question, in this study we used model NCs addressed to each one of the three main routes associated with endothelial transcytosis (clathrin-, caveolae-, and CAM-mediated pathways) by respectively targeting TfR, PV1, and ICAM-1 in both ASM-normal *vs*. ASM-deficient BBB models. This shall help to determine the effects of NPD on endothelial transcytosis and comparatively determine the most promising candidate routes to deliver ERT to the CNS in this disease.

## 2 MATERIALS AND METHODS

### 2.1 Antibodies and Reagents

$^{125}$Iodine ($^{125}$I) was from Perkin Elmer (Waltham, MA), Iodination Tubes were from Pierce (Waltham, MA, USA), Bio-Spin P-30 Gel Tris Columns were from Bio-Rad (Hercules, CA, USA), L-glutamine, 4′,6-Diamidino-2-phenylindole (DAPI), and 10 kDa Texas Red dextran were from Fisher Scientific (Hampton, NH, USA). Trichloroacetic acid (TCA), bovine serum albumin (BSA), Triton X-100, and imipramine hydrochloride were from Sigma Aldrich (St. Louis, MO, USA). RPMI cell medium and fluorescent secondary antibodies (Abs) were from Life Technologies (Carlsbad, CA, USA). Anti-VE-cadherin, Amplex Red Sphingomyelinase kit, and BODIPY-Fl$_{C12}$-sphingomyelin were from Thermo Fisher (Waltham, MA, USA). Anti-claudin-5 was from Abcam (Cambridge, UK). Endothelial cell growth supplement (EGCS), heparin, and anti-TfR were from Merck (Darmstadt, Germany). Polystyrene Fluoresbrite™ beads (0.1 µm, green-fluorescent) were from Polysciences (Warrington, PA, USA). Human brain microvascular endothelial cells (HBMECs) were from Innoprot (Derio, Spain). Transwell inserts (1.0 µm-pore) were from Corning (NY, USA). Recombinant human tumor necrosis alpha (TNFα) was from Novus Biologicals (Littleton, CO, USA). Anti-ICAM-1 Ab was produced from hybridoma HB-9580 (ATCC, Manassas, VA, USA). Plasmalemma vesicle associated

protein-1 (PV1) Ab was from Antibodies-online (Aachen, Germany). Control mouse IgG was from Vitro (Seville, Spain). Paraformaldehyde (PFA) was purchased from Aname (Madrid, Spain).

### 2.2 Radiolabeling of antibodies

Where indicated, Abs were labelled with $^{125}$I, as described[66]. For this purpose, 1 mg/mL Ab was incubated for 5 min at 4 °C with 20 μCi $^{125}$I using Pierce Iodination Tubes. Then, Bio-Spin Columns were used to remove free $^{125}$I by centrifugation for 4 min at 1000 x g at room temperature (RT). $^{125}$I-Ab specific activity was then assessed by quantifying the protein content using Bradford assay and $^{125}$I counts per minute (CPM) using a gamma counter, before and after separating free $^{125}$I from the $^{125}$I-Ab preparation by TCA precipitation and centrifugation, as described[66]. The specific activity was calculated as follows:

$$Specific\ activity\ \left(\frac{CPM}{\mu g}\right) = \frac{Radioactive\ counts\ in\ protein\ (\frac{CPM}{ml})}{Protein\ concentration\ (\frac{\mu g}{mL})}$$

### 2.3 Preparation, characterization, and stability of model nanocarriers

Fluorescent polystyrene beads (0.1 μm) were coated by surface adsorption with Abs, as described[30,36]. Briefly, 7000 μg/mL NCs were mixed for 1 h at RT with 1.5 μM total Ab (1/2 specific Ab + 1/2 non-specific IgG in the case of targeted NCs, or full amount corresponding to non-specific IgG for control NCs), a concentration that favors outward display of Abs[67]. Preparations where then centrifuged at 12000 rpm for 3 min to remove non-coated Abs and NC pellets were resuspended in 1% BSA in PBS, sonicated, and tested for their hydrodynamic diameter, polydispersity index (PDI), and ζ-potential by dynamic light scattering (DLS; Zetasizer Ultra, Malvern Instruments; Westborough, MA). The number of Ab molecules per NC was assessed from the $^{125}$I-Ab label in NC pellets, as follows:

$$\boldsymbol{Antibody\ \left(\frac{molecules}{NC}\right) = \frac{\frac{CPM\ pellet\ \times N}{Specific\ acitvity\ \left(\frac{CPM}{\mu g}\right) \times MW}}{Number\ of\ NCs}}$$

Where, N = Avogadro's number, Ab MW = 150,000 Da, number of NCs was provided by vendor and verified by DLS, and the specific activity was calculated as described in section 2.2.

Additionally, the stability of the coat was assessed by incubating anti-ICAM-1 NCs for 5 h in complete cell medium containing 10% fetal bovine serum (FBS), after which NCs were separated from potentially released Ab molecules by centrifugation, followed by quantification in a gamma counter, as described above. An additional test to verify the integrity of the NC $^{125}$I-Ab coat during 24 h in cellular experiments is described in section 2.12.

### 2.4 Cellular blood-brain barrier models

The sources for HBMECs (hereafter called brain ECs) and all reagents involved in cell culture are listed in section 2.1. Cells were grown on 1.0 μm-pore transwell inserts for 7 days at 37°C, 5% $CO_2$, and 95% relative humidity in RPMI supplemented with 10% FBS, 2 mM L-glutamine, 30 μg/mL ECGS, 100 μg/mL heparin, 100 U/mL penicillin, and 100 μg/mL streptomycin, as described[30,36]. To mimic inflammation, an NPD hallmark[4], cells were incubated with 10 ng/mL TNFα overnight prior to experiments[30,34]. To mimic NPD, cells were treated with TNFα (as above) and, additionally, 20 μM imipramine for 48 h to induce ASM deficiency and cause aberrant storage of sphingomyelin as in NPD[68].

### 2.5 ASM activity

The Amplex Red Sphingomyelinase kit was used to measure ASM activity, as described[62]. This test is based on incubation of cell lysates with sphingomyelin substrate and a multi-enzyme chain-reaction to produce fluorescent resorufin, which is measured using a spectrofluorometer at 571 nm excitation and 585 nm emission.

In addition, cells were incubated overnight with BODIPY-$Fl_{C12}$-sphingomyelin to allow it to incorporate into cell membranes. This is a fluorescent substrate analogue for ASM and can, thus, be used to determine substrate accumulation in cells that are treated with imipramine to become ASM deficient. Then, cells were washed in PBS, fixed with 2% PFA, mounted on glass slides, and imaged by fluorescence microscopy under the green channel, as indicated[34].

### 2.6 Cell junction staining

As described[30,69], brain ECs were fixed with 2% PFA and incubated at RT with either 3 μg/mL anti-VE-cadherin for 1 h or 1:50 dilution anti-claudin-5 for 16 h, and then washed in PBS. Samples were then incubated for 30 min with 4 μg/mL fluorescent secondary Ab and 2 μg/mL DAPI for nuclear staining. Cells were finally washed with PBS, mounted on slides, and imaged using the LSM 800 confocal microscope and either 63X or 10X objectives, respectively, from Zeiss (Jena, Germany).

### 2.7 Cell barrier permeability

As described[69], to verify the barrier function, brain EC monolayers were incubated for 30 min (the incubation pulse used in transcytosis experiments) with either $^{125}$I-Ab NCs or 10 kDa Texas Red dextran added on the AP side, so that their leakage to the BL chamber could be determined. Alternatively, to further validate the barrier function in experiments aimed to examine NC re-uptake after transcytosis, 10 kDa Texas Red dextran was added for 30 min at the BL side. In both cases, the

concentration of each of these components was analyzed in both AP and BL sides using a gamma counter to detect $^{125}I$ or a spectrofluorometer to detect Texas Red dextran (excitation/emission 580/604 nm), respectively. Data were used to calculate the permeability coefficient ($P_{app}$) as follows:

$$P_{app} = \frac{dQ}{dt} x \frac{1}{A\ x\ C_0}$$

Where, dQ/dt = the amount of apically-added 10 kD Texas Red dextran or NCs (for the number of NCs, see section 2.3) present in the BL side as a function of time (mg/s or NCs/s, respectively), A = area of the transwell, and $C_0$ = initial concentration of dextran or NCs added to the AP side.

### 2.8 Receptor expression

Brain ECs were detached using trypsin, collected by centrifugation, and incubated for 1 h at RT with 2 µg/mL primary Abs that specifically bind to ICAM-1, TfR, or PV1. Then, cells were washed and incubated with Alexa Fluor 488 or Alexa Fluor 405 labeled secondary Abs at 1.5 µg/mL for 30 min. Cells were trypsinized before the incubation with Abs because trypsin might also cleave bound Abs and, thus, generate artefacts. Cell were then washed and analyzed using the Gallios flow cytometer and FlowJo software (Beckman Coulter; Pasadena, CA, USA). As published[69], relative expression of cell-surface markers was calculated as follows:

$$Relative\ expression = \frac{Receptor\ signal\ (specific\ antibody)}{Background\ signal\ (non-specific\ IgG)}$$

where, Signal = the fraction of the cell population expressing a cell-surface marker multiplied by the expression level found (mean fluorescence intensity), to better reflect the relative expression of each marker in the full cell population.

### 2.9 Nanocarrier specific binding to cells

Brain ECs were incubated for 60 min with green-fluorescent NCs added over the cells. As a note, since these binding (section 2.9) and uptake tests (section 2.10) used microscopy analysis, which is less sensitive than the radiotracing method used for permeability (section 2.7) and transcytosis tests (section 2.11), a longer NC incubation time was employed (60 min *vs.* 30 min). Thereafter, cells were washed twice with PBS to remove non-bound NCs, fixed, mounted on slides, and imaged by fluorescence microscopy. As described[30,70], the number of NCs per cell was assessed using a custom algorithm in ImagePro (Media Cybernetics, Rockville, Maryland, USA), which recognizes NC-sized fluorescent spots surrounded by background fluorescence.

### 2.10 Cellular uptake of nanocarriers from the apical chamber

Brain ECs were incubated for 60 min with green-fluorescent NCs at 37 °C added over the cells. Then, non-bound NCs were washed off by adding and removing twice 1 ml PBS. Next, cells were fixed and then incubated for 30 min with red Alexa Fluor 555-conjugated secondary Ab targeted to the primary Ab on the NC surface. This established method[30,70] differentially marks cell surface-bound NCs as yellow (green + red) *vs.* internalized NCs as green, which can be quantified by fluorescence microscopy using a customized algorithm[30,70]. The uptake mechanism for anti-ICAM-1 NCs was similarly tested, except that the experiment was conducted in the presence of 3 mM amiloride, known to inhibit CAM-mediated endocytosis[33].

### 2.11 Nanocarrier transcytosis across cells

As published[30,69], brain EC monolayers were incubated at 37 °C with $^{125}$I-Ab coated NCs added to the AP chamber using a 30 min pulse, followed by removing NCs by washing cells twice with PBS. At this time, the $^{125}$I-content of the cellular fraction was assessed using a gamma counter to calculate the total number of NCs that originally interacted with receptors during the pulse period. Cells were then incubated in NC-free cell media for the indicated chase times up to 24 h, to allow transport of pre-bound NCs. Next, the BL fraction was collected and its $^{125}$I-content quantified to calculate the percent of transcytosis from the original number of NC interacting with cells at 30 min. This ensures the tracing of receptor-mediated transport, avoiding confounding results from any passive apical piggybacking of NCs. The absolute number of NCs in each fraction and the rate of transcytosis (% transcytosis), were calculated as follows:

$$Number\ of\ NCs\ in\ a\ fraction = \frac{CPM\ in\ the\ fraction}{\frac{CPM}{NC}}$$

$$\%\ Transcytosis = \frac{BL\ NCs\ at\ given\ time}{Cellular\ NCs\ at\ 30\ min}$$

Where the number of NCs was provided by the vendor and empirically verified by DLS, and CPM/NC had been obtained using the data shown in the equation in section 2.3.

### 2.12 Integrity of Ab coated nanocarriers during cellular experiments

To ensure $^{125}$I remained on NCs measured in section 2.11, a control was performed comparing the transcytosis of NCs coated with anti-ICAM-1:$^{125}$I-IgG *vs.* $^{125}$I-anti-ICAM-1:IgG (1:1 molar ratio). Since the specificity of anti-ICAM-1 NCs *vs.* IgG NCs had been established through section 2.9 experiments, similar transcytosis for both formulations would only be possible if $^{125}$I would remain on Ab coated on NCs, as shown[30].

In addition, NCs transcytosed to the BL side were analyzed by DLS and compared to those originally added to the AP side, as well as controls non-coated NCs and also complete cell medium without NCs, as published[69].

### 2.13 Lysosomal transport of nanocarriers by brain endothelial cells

Brain ECs grown to confluency on transwells were incubated for 40 min with Texas Red dextran (10 kDa) to allow its fluid-phase uptake. Dextran was then washed off in PBS and cells were incubated for 1 h in dextran-free cell medium, to allow internalized dextran to travel to lysosomes. Then, cells were incubated for 30 min with green-fluorescent NCs, washed, and incubated with NC-free cell medium for the indicated times. Next, samples were fixed and imaged by fluorescence microscopy to quantify the number of green NCs colocalizing with red dextran-positive lysosomes (yellow), as described previously[30].

### 2.14 Basolateral reuptake of nanocarriers following transcytosis

First, brain ECs were incubated for 30 min with green-fluorescent anti-ICAM-1 NCs added to the AP chamber, then washed to remove non-bound NCs. Cells were further incubated with NC-free cell medium for 30 min simultaneously to adding 10 kDa Texas Red dextran to the BL chamber, to distinguish respective dextran-positive BL fluid phase from the dextran-negative AP fluid phase. Thus, when NCs transcytose from the AP side to the BL side of the cell monolayer, if they were taken up by cells again before moving to the BL chamber below the filter, dextran-positive fluid phase would enter the same NC-positive endocytic vesicle and be visualized as colocalization of green NCs + red dextran (yellow) by fluorescence microscopy. As a control, cells were first incubated with BL Texas Red dextran so that it could enter cells alone, then washed to remove extracellular dextran, and finally NCs were added on the AP side as described above. In this case, NCs and dextran would be expected in different endocytic vesicles (no colocalization), for which this assay can determine whether BL re-uptake of NCs takes place.

Second, once BL re-uptake was found, quantification of NC uptake from the BL chamber was assessed using a similar dextran-free method as described in section 2.10. For this, NCs were added to the BL chamber for a 30 min binding pulse, followed by wash-removal of NCs with PBS and uptake chases up to the indicated time points. Finally, NCs bound to the BL cell surface were distinguished by fluorescence microscopy from those internalized from the BL side by counterstaining them with a red-labeled secondary antibody (red + green = yellow *vs.* green alone), as described in section 2.10.

### 2.15 Statistics

Data were calculated as average ± standard error of the mean (SEM). Regarding independent experiments, for fluorescence microscopy $n \geq 3$, for radiotracing $n \geq 4$, and for flow cytometry $n = 3$. Statistical significance was determined as $p<0.05$ by either Student's t-test for two-groups comparisons or one-way ANOVA followed by Tukey's as a multiple comparison test.

## 3 RESULTS AND DISCUSSION

### 3.1 Disease model validation and nanocarrier characterization

The goal was to comparatively evaluate NCs targeted to each of the three known routes of endothelial transcytosis (clathrin-, caveolae-, and CAM-mediated pathways) in an NPD cell model, for which TfR, PV1, and ICAM-1 were selected as cell-surface markers of respective pathways[32,45,51,52]. First, ECs were grown to confluency on transwells and incubated with both TNFα and imipramine, to respectively mimic inflammation and ASM-deficiency, both characteristic of NPD[4]. Instead, cells treated with TNFα alone to mimic inflammation only, served as an ASM-normal model. These models were confirmed by quantifying the ASM activity of respective cell lysates using a commercial kit (figure 1a), showing decreased enzyme activity in the NPD model. Conversely, microscopy visualization showed increased cellular accumulation of BODIPY-$Fl_{C12}$-sphingomyelin, a fluorescent ASM substrate analogue, in the NPD model (figure 1b).

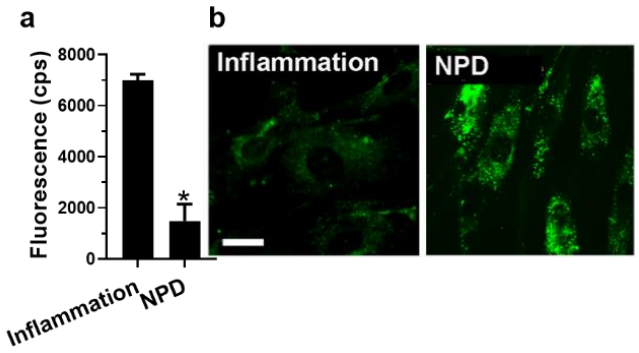


**Figure 1** ASM-deficient cell model. ECs were incubated at 37 °C with TNFα + imipramine to simulate inflammation + ASM deficiency as in NPD, or just with TNFα to simulate inflammation alone (hence, ASM-normal). (a) Cell lysates were incubated for 1 h at 37 °C with the Amplex Red Sphingomyelinase kit, which detects ASM activity by rendering fluorescent resorufin, ultimately measured by spectrofluorometry (cps = counts per second). Data are average ± SEM. *$p < 0.05$ by Student's t test. (b) Cells were incubated overnight with BODIPY-$Fl_{C12}$-sphingomyelin, a fluorescent ASM substrate analogue, then washed, fixed, and imaged by fluorescence microscopy under the green channel. Scale bar = 10 μm.

Next, using untreated cells as controls, flow cytometry showed modest expression levels for TfR, lower expression for ICAM-1, and negligible PV1 expression in control untreated brain ECs (figure 2). This

is in line with the literature on ICAM-1 baseline expression in control ECs[32,71] and downregulation of caveoli in healthy BBB[45,49], while comparatively higher TfR expression was anticipated based on its iron homeostasis function[44,69]. As expected, due to its well-known association with inflammation[32,71], TNFα markedly increased ICAM-1 expression, slightly decreased that of TfR and did not change that of PV1 (figure 2a, b). Treatment with both TNFα + imipramine to mimic NPD further increased ICAM-1 expression to very high levels, modestly increased PV1, and slightly increased TfR compared to the TNFα-alone condition (figure 2a, b). Given this, ICAM-1 was the most highly expressed marker compared to TfR and PV1 both in the inflammation and NPD models, followed by TfR and last PV1 (figure 2). To our knowledge, there are no previous data on how ASM deficiency *per se* alters these markers, since most available results are from cellular and animal models where ASM deficiency occurs simultaneously to inflammation[4,53].

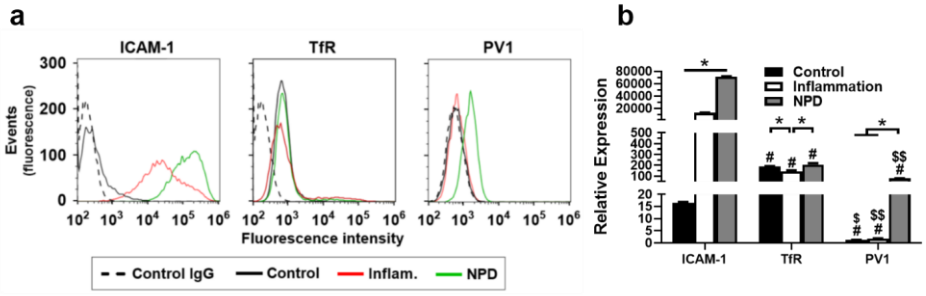


**Figure 2** Expression of cell-surface markers. (a) Flow cytometry quantification of the expression of ICAM-1, TfR, and PV1 using specific antibodies (Abs) *vs.* control IgG, on brain ECs that had been incubated in control cell medium, cell medium containing TNFα + imipramine to simulate inflammation + ASM deficiency as in NPD, or TNFα to simulate inflammation alone (ASM-normal). Dashed line = control IgG, solid black line = control cells, red line = inflammation condition, green line = NPD condition. (b) Relative expression of cell-surface markers calculated using data from FlowJo® software, taking into consideration both the fraction of cells expressing each marker as well as their expression level, as described in section 2.8. Data are average ± SEM. *Compares the same marker in all three different conditions; #compares PV1 or TfR to ICAM-1, within each particular condition; $ or $$ compare PV1 to TfR within each particular condition ($p<0.05$) by one-way ANOVA ($) or Student's *t* test ($$).

Since this NPD model expressed all three markers, model NCs targeting each of them were prepared. Polystyrene NCs were used as they are not biodegradable and this avoids problems during long cellular experiments. Validating this NC model, we have demonstrated that targeted polystyrene nanoparticles behave similarly to targeted PLGA NCs in terms of size, PDI, ζ-potential, cellular transport, and *in vivo* biodistribution[31,36,69,72]. Pristine polystyrene NCs had 114 nm mean diameter, 0.03 PDI, and -25 mV ζ-potential (table 1). Targeted NCs were coated with $^{125}$I-Abs specific for ICAM-1, TfR, or PV1 mixed at 1:1 molar ratio with non-specific IgG, while control NCs were coated with double dose non-specific $^{125}$I-IgG to keep total Ab/NC similar among all formulations (see section 2.3). Ab coating increased NC size up to 180–207 nm, PDI up to 0.14–0.16, and ζ-potential up to -23 –-19 mV (table 1). All formulations had comparable coating, *i.e.* 200 $^{125}$I-IgG molecules/NC for the control

formulation and 81-97 specific $^{125}$I-Ab molecules/NC for targeted formulations (notice that this number is about half because the half corresponding to non-specific IgG was not traced; table 1). Taking into account the measured size of the core polystyrene NC and a 14.5 nm circle-diameter occupancy (either for standup or flat projections) for this type of Ab, this amount of coated Ab molecules should distribute as a single layer on the NC surface. Importantly, 90±2% of the protein coat remained on the NC surface after 5 h incubation in serum-supplemented cells medium, as determined using anti-ICAM-1 NCs as an example (not shown), and incubation with cells for up to 24 h under physiological conditions, described thereafter in section 3.3, further validated the Ab coat stability.

**Table 1** NC characterization

| Formulations | Coat | Size | PDI | ζ-potential | Ab mol./NC[a] |
|---|---|---|---|---|---|
| **Polystyrene beads** | - | 114.00±0.58 | 0.03±0.00 | -25.20±0.84 | - |
| **Anti-ICAM-1 NCs** | $^{125}$I-anti-ICAM-1/IgG ($\frac{1}{2}+\frac{1}{2}$) | 207.30±4.37 * | 0.16±0.01 * | -21.68±1.92 | 97.57±6.83 # |
| **Anti-TfR NCs** | $^{125}$I-anti-TfR/IgG ($\frac{1}{2}+\frac{1}{2}$) | 195.78±4.44 * | 0.15±0.01 * | -20.57±2.72 | 81.69±3.15 # |
| **Anti-PV1 NCs** | $^{125}$I-anti-PV1/IgG ($\frac{1}{2}+\frac{1}{2}$) | 180.22±3.06 *$ | 0.14±0.01 * | -23.83±2.07 | 85.56±6.78 # |
| **IgG NCs** | IgG (1) | 199.50±13.85 * | 0.18±0.02 * | -19.35±0.35 | 200.22±5.52 |

Ab = antibody; molec. = molecule; NC = nanocarrier; PDI = polydispersity index.
[a] Targeted NCs had a coat consisting of 1/2+1/2 mixture of specific $^{125}$I-Ab+non-specific IgG, while control $^{125}$I-IgG NCs were coated fully with $^{125}$I- IgG; hence double amount of traceable Ab molecules per NC is expected.
Data are average ± SEM. *Compares each coated NC *vs.* non-coated NCs (polystyrene beads); #compares each targeted NC to IgG NCs; $compares each targeted NC to anti-ICAM-1 NCs ($p<0.05$ by one-way ANOVA).

Then, the specificity of targeted NCs was verified in brain ECs by fluorescence microscopy, showing good specificity compared to control IgG NCs (figure 3). For instance, in TNFα-treated cells (inflammation model), the highest specificity was achieved using anti-ICAM-1 NCs, followed by anti-TfR NCs and finally anti-PV1 NCs, with 61.1-, 16.3-, and 2.7-fold increase over IgG NCs, respectively. This result aligns with respective expression levels discussed above.

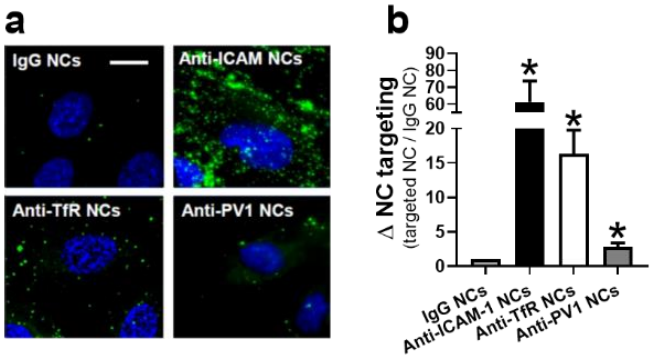


**Figure 3** NC targeting specificity. (a) TNFα-treated brain ECs (inflammation model) were incubated for 1 h with green-fluorescent NCs targeted to either ICAM-1, TfR, or PV1, or with non-targeted IgG NCs. Cells were then washed, fixed, and analyzed by fluorescence microscopy. Blue = cell nuclei stained with DAPI. Scale bar = 10 µm. (b) Quantification of NCs per cell, expressed as fold increase (Δ) over IgG NCs. The ratio was calculated by dividing the number of NCs counted

on each individual cell for each targeted formulation by the average number of NCs/cell found for the non-specific IgG NC formulation. *Compares NCs/cell for each targeted formulation to NCs/cell for IgG NCs ($p<0.05$ by Student's t-test).

### 3.2 Disease effect on nanocarrier binding and uptake in brain endothelial cells

After the previous validations, the role of disease on NC binding was analyzed by fluorescence microscopy (figure 4a). Under control condition (figure 4b), anti-ICAM-1 NCs and anti-TfR NCs bound to cells comparably (99.0 and 89.3 NCs/cell), whereas anti-PV1 NCs bound much less (39.9 NCs/cell). Lower binding was expected for anti-ICAM-1 NCs *vs.* anti-TfR NCs based on their relative expression levels in this condition, suggesting that the longer extracellular domain of ICAM-1 may be more accessible to NCs, as previously reported[37]. Inflammation increased the total binding of anti-ICAM-1 NCs and anti-TfR NCs by 5-fold and 1.5-fold, but not that of anti-PV1 NCs (figure 4c), so that their absolute binding levels were 494.3, 131.4, and 42,4 NCs per cell, respectively (figure 4d). These relative binding levels are aligned with respective marker expression data discussed above. Yet, an increase was not expected for anti-TfR NCs based on TfR expression, suggesting that inflammation may change the distribution of this receptor, speculatively. Comparative results were found in control condition in a recent publication, although that study had used ganglioside GM1 instead of PV1 as a caveolar marker and PLGA NCs instead of polystyrene models[69]. Yet, that study did not investigate respective effects of inflammation, for which data presented here completes and extends previous information.

Then, cells were treated with both TNFα + imipramine[68] to mimic NPD (figure 4a). Compared to control condition, the binding of anti-ICAM-1 NCs and anti-TfR NCs were increased by 7.3-fold and 1.8-fold, respectively (figure 4e). For anti-ICAM-1 NCs, this result is in line with increased receptor expression, while this is not the case for TfR. Yet, as speculated in the previous case, this increase could be due to a change in TfR accessibility caused by TNFα included in this condition. Anti-PV1 NCs binding was not affected while its expression had been. Since PV1 resides in caveoli[51] and ASM deficiency alters the lipid composition of membranes, especially affecting lipid-rafts[73], this result might be explained if the NPD condition alters PV1 display on the plasma membrane or its accessibility for NCs binding[74–76]. When comparing NPD to inflammation to assess the specific effect of ASM deficiency (figure 4f), only anti-ICAM-1 NCs binding increased (1.5-fold), which is in line with receptor expression data and the possible effect of this deficiency on PV1 accessibility discussed[74–76]. Overall, the comparative binding of anti-ICAM-1 NCs, anti-TfR NCs, and anti-PV1 NCs in NPD was 726.7, 162.2, and 45.2 NCs per cell, respectively (figure 4g), suggesting that ICAM-1 might be a privileged marker for NC targeting in this disease.

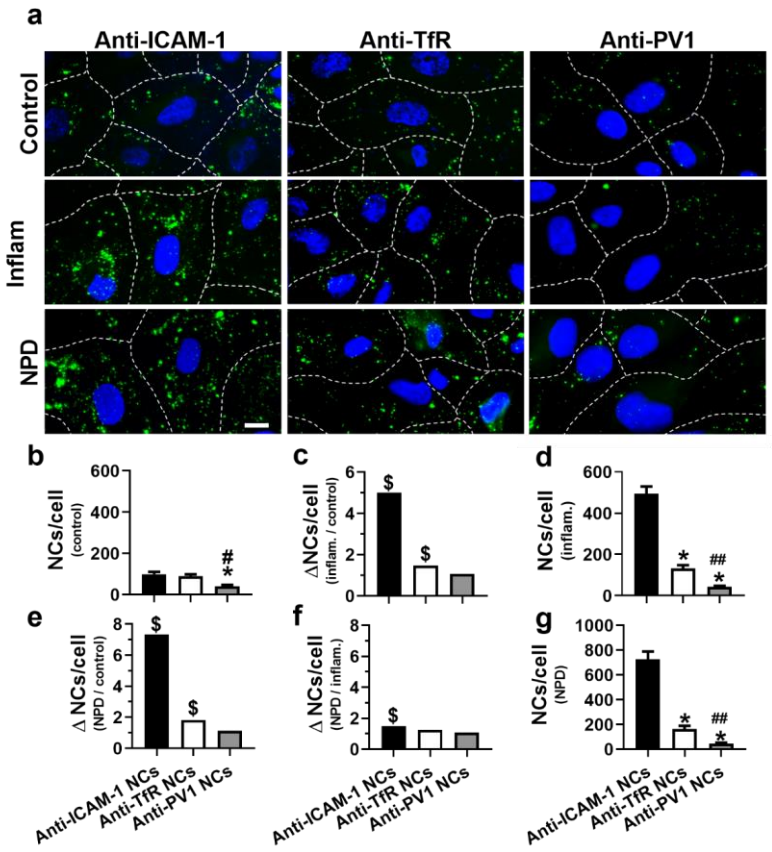


**Figure 4** NC binding to brain ECs under control, inflammation, and NPD conditions. Brain ECs grown to confluency on transwells were left untreated (control), treated with TNFα to mimic inflammation (Inflam.), or treated with both TNFα + imipramine to mimic NPD. Then, cells were incubated for 1 h with green-fluorescent NCs, washed to remove non-bound NCs, fixed, and analyzed by fluorescence microscopy. (a) Representative micrographs. Green = NCs, blue = nuclei stained with DAPI; dashed lines = cell borders. Scale bar = 10 µm. (b,d,g) NCs per cell (NCs/cell) under (a) control condition, (d) inflammation, and (g) NPD. (c,e,f) fold change (Δ) in the number of NCs/cell in (c) inflammation over control condition, (e) NPD over control, or (f) NPD over inflammation. Data are average ± SEM. (b,d,g) *Compares anti-TfR NCs or anti-PV1 NCs to anti-ICAM-1 NCs ($p<0.05$ by one-way ANOVA); # or ## compare anti-PV1 NCs to anti-TfR NCs ($p<0.05$ by one-way ANOVA (#) or Student's *t* test (##)). (c,e,f) $Compares NC/cell in the numerator condition *vs.* the denominator condition ($p<0.05$ by Student's t-test).

Subsequently to binding, NC uptake by cells was investigated by fluorescence microscopy (figure 5a). Under control condition (figure 5b), no difference between anti-ICAM-1 NCs and anti-TfR NCs uptake

rate was found at 1 h, whereas anti-PV1 NCs uptake rate was higher, *i.e.* 30.7%, 36.3%, and 50.5% of all NCs interacting with cells, respectively. Inflammation did not affect this parameter for any NCs tested (figure 5c), resulting in similar uptake rates as for control condition (figure 5d). A similar result was previously reported for anti-ICAM-1 NCs in brain ECs and other cell types and for anti-TfR NCs in non-brain endothelial cells[37,41,77], while this information is missing for anti-TfR NCs in brain ECs and anti-PV1 NCs on any cell type. However, inflammation increased the absolute number of anti-ICAM-1 NCs internalized per cell by 6.2-fold, as reported[41,77], but did not change that of anti-TfR NCs or anti-PV1 NCs (figure 5e,f). Hence, that overall respective absolute number of NCs internalized per cell was 174.6, 45.6, and 22.2 in inflammation (figure 5g), in accordance with receptor expression and NC binding. Thus, it seemed these two parameters better defined absolute intracellular transport, rather than the uptake rate.

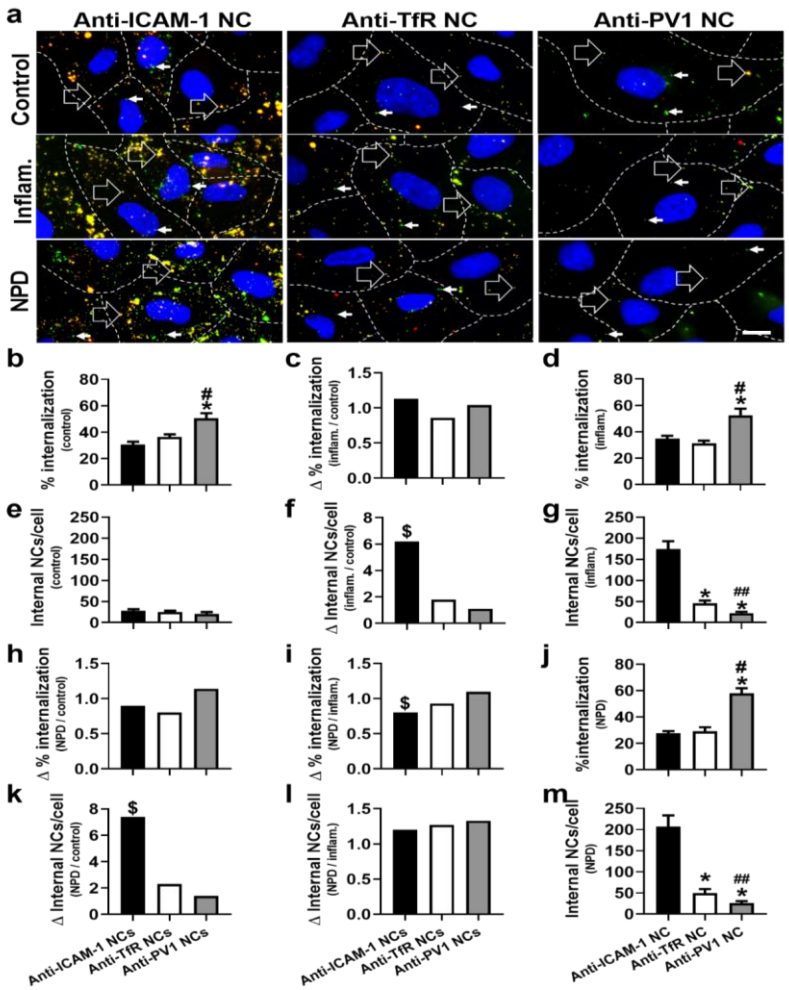


**Figure 5** NC uptake by brain ECs under control, inflammation, and NPD conditions. Brain ECs grown to confluency on transwells were left untreated (control), treated with TNFα to mimic inflammation, or treated with both TNFα + imipramine to mimic NPD. Then, cells were incubated for 1 h with green-fluorescent NCs, washed to remove non-bound NCs, fixed, and cell-surface bound NCs were counterstained with red-fluorescent secondary antibody to distinguish internalized NCs (green alone) from bound NCs (green + red = yellow) by fluorescence microscopy. (a) Representative micrographs. Blue = nuclei stained with DAPI; dashed lines = cell borders. Scale bar = 10 μm. (b,d,j) Uptake rate quantified as % internalized NCs of the total NCs interacting per cell in (b) control, (d) inflammation, and (j) NPD conditions. (c,h,i) Fold change (Δ) in the rate of NC uptake in (c) inflammation compared to control, (h) NPD compared to control, or (i) NPD compared to inflammation. (e,g,m) Absolute number of NCs internalized per cell in (e) control, (g) inflammation, and (m) NPD conditions. (f,k,l) Δ in the rate of NC uptake in (f) inflammation compared to control, (k) NPD compared to control, or (l) NPD compared to inflammation. Data are average ± SEM. (b,d,e,g,j,m) *Compares anti-TfR NCs or anti-PV1 NCs to anti-ICAM-1 NCs; # or # compare anti-PV1 NCs to anti-TfR NCs ($p<0.05$ by one-way ANOVA (#) or Student's *t* test (##)). (c,f,h,i,k,l) $Compares NC/cell in the numerator condition *vs.* the denominator condition ($p<0.05$ by Student's t-test).

Finally, NC uptake was assessed for ASM deficiency in NPD (figure 5a). This model decreased by 20% the uptake rate for anti-ICAM-1 NCs compared to the inflammation condition (figure 5i). This was expected because ASM-mediated generation of ceramide at sites of ICAM-1 engagement on the plasma membrane support engulfment and cytoskeletal reorganizations through the CAM-pathway[78]. Instead, the uptake rate did not change for the other two formulations. Regarding the absolute number of NCs internalized per cell, NPD neither varied this parameter for anti-TfR NCs or anti-PV1 NCs compared to inflammation or control condition (figure 5k,l), but it increased for anti-ICAM-1 NCs compared to control (7.4-fold; figure 5k). However, this effect was due to the inflammation component of NPD, since no difference was observed between these two conditions (figure 5l), and this relates to the observed TNFα-induced ICAM-1 overexpression. Hence, although ASM deficiency decreased the rate of anti-ICAM-1 NC uptake, their increased binding compensated this fact and the absolute number of anti-ICAM-1 NCs per cell did not vary in NPD (figure 5m). Overall, anti-ICAM-1 NCs significantly surpassed anti-TfR NCs and anti-PV1 NCs regarding absolute uptake levels, *i.e.* 207.2, 57.8, and 29.5 NCs internalized per cell, respectively, in the NPD model (figure 5m), in accordance with receptor expression and NC binding.

Interestingly, some of these data were unexpected based on literature. For instance, a reduction of clathrin- and caveolae-mediated endocytosis has been reported in NPD macrophages and fibroblasts[62–65], for which a reduction in the uptake of anti-TfR NCs or anti-PV1 NCs had been expected in this study. However, the former studies focused on natural ligands, such as transferrin or cholera toxin B, but not multivalent NCs. Since these NCs display a high number of targeting Abs and this has been shown to increase NC avidity[72], their stronger receptor engagement may compensate small changes in the ability to induce endocytosis caused by NPD. Furthermore, the cited studies used macrophages[64] or fibroblasts[62,63] *vs.* brain ECs in this study, all of which have different functions in the body and only ECs serve as barriers to separate compartments and transport cargo *via* transcytosis[45,49].

### 3.3 Disease effect on nanocarrier transcytosis across brain endothelial cells

The described results suggest that ICAM-1 NCs might provide an advantage for brain delivery in inflammation and NPD compared to those targeting TfR or PV1. However, transcytosis additionally depends on transport across cells and BL secretion; thus, increased binding or uptake may not ensure transcytosis if NCs get trapped within cells. Therefore, AP-to-BL transcytosis was studied. First, the presence between adjacent cells of VE-cadherin and claudin-5, markers of confluent endothelium and brain endothelium, respectively, was verified by microscopy (figure 6a). This indicated the presence of cell-cell junctions between adjacent brain ECs in these monolayers, as in previous studies[30,69]. In fact, no AP-to-BL leakage of fluorescent dextran was observed, validating barrier function: *i.e.* $5x10^{-6}$ cm/s Papp (figure 6b), equivalent to ≥ 99% dextran concentration added to the AP side remaining at this location (supplemental figure S1). As such, this cellular model prevented targeted NCs from leaking into the BL chamber upon their AP incubation for 30 min, which is the maximum time used thereafter to incubate NCs in the AP chamber: *i.e.* $7.6x10^{-6}$, $6.3x10^{-6}$, and $8.36x10^{-6}$ cm/s Papp for anti-ICAM-1 NCs, anti-TfR NCs, and anti-PV1 NCs, respectively (figure 6b), which is equivalent to ≥ 97.5% of all NCs remaining in the AP chamber (supplemental figure S2), while in the absence of cells

only 76.3% remained at this location (supplementary figure S3). These data paired well with previous publications using this model[30,69], validating it.

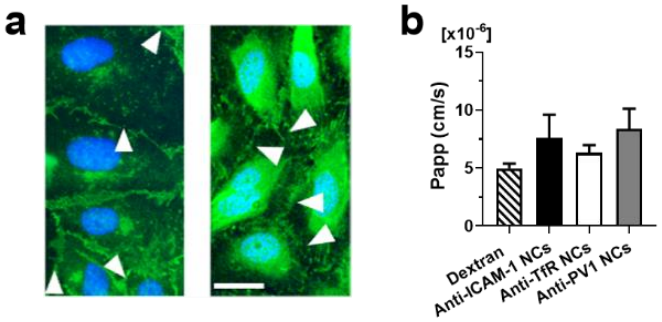


**Figure 6** Barrier function of brain EC monolayers. TNFα-treated brain EC monolayers (inflammation) grown for 7 days to confluency on transwell filters. (a) Cells were fixed, permeabilized, immunostained for either VE-cadherin or claudin-5 (green) and cell nuclei were labeled with blue DAPI, then visualized by fluorescence microscopy. Arrowheads = VE-cadherin or claudin-5 at cell-cell junctions. Scale bar = 10 µm. (b) Cells were incubated for 30 min with Texas Red dextran (10 kDa) or with $^{125}$I-antibody coated NCs targeted to either ICAM-1, TfR, or PV1, all added to the apical (AP) chamber. Then dextran or NCs were measured at both the AP and basolateral (BL) chambers by either spectrofluorometry (dextran) or gamma counting (NCs), from which the permeability coefficient (Papp) was calculated. Data are average ± SEM.

Next, transcytosis was tested, for which cells were incubated with NCs for 30 min to allow binding, then NCs were removed from the AP and BL chambers and cells were incubated with NC-free medium to particularly trace NCs pre-bound to cells and ensure receptor-mediated transport. For precise quantification, we traced $^{125}$I-label on the Ab coating the NCs, for which the integrity of formulations was verified. For instance, DLS demonstrated the same size for $^{125}$I-Ab NCs added to the AP chamber and harvested from the BL side after transcytosis, both similarly larger than non-coated NCs (supplementary figure S4a). Furthermore, quantifications of NCs interacting with cells or transported to the BL chamber were the same when using formulations coated with Ab+$^{125}$I-IgG or $^{125}$I-Ab+IgG (supplementary figure S4b). Since IgG does not interact with cells (figure 3), this demonstrates that $^{125}$I-Ab fully remains on the NC coat during experiments.

A previous publication showed that NCs targeted to all three routes could transcytose in control untreated cells[69]. Among them, caveolae-targeted NCs performed best compared to clathrin-targeted or CAM-targeted NCs, which showed similar transcytosis rate under this condition[69]. Treatment with both TNFα + imipramine to mimic NPD led to a transcytosis decrease for clathrin- and caveolae-targeted NCs but increased that of CAM-targeted NCs[69]. However, whether this change was due to inflammation or ASM deficiency alone was unknown. To clarify this, in this study inflammation (TNFα alone) was compared to NPD (TNFα+imipramine) to discern the role of enzyme deficiency on this transport (figure 7). Despite small visual differences (anti-TfR NCs being the fastest in inflammation and slowest in NPD; figure 7a), all three targeted formulations transcytosed to the BL chamber at rates statistically comparable: *e.g.* by 24 h, 59%, 60%, and 55% of all pre-bound NCs were transcytosed in inflammation and 53%, 45%, and 60% in NPD (figure 7a). However, the absolute levels

of transcytosed NCs amply varied among them (figure 7b). For instance, at 24 h in inflammation we found $9.7x10^7$, $3.5x10^7$, and $4.8x10^7$ NCs transcytosed per well for anti-ICAM-1 NCs, anti-TfR NCs, and anti-PV1 NCs, respectively, and their levels were $5.8x10^7$, $2.9x10^7$, and $1.3x10^7$ NCs/well in NPD. Therefore, at such comparable transcytosis rates, absolute transcytosis seemed governed by the level of marker expression and NC binding, making anti-ICAM-1 NCs the most favorable formulation in both inflammation and NPD. This outcome pairs well with previous publications showing increased brain targeting after *i.v.* administration of polymer NCs addressed to ICAM-1 *vs.* TfR or ganglioside GM1 in mouse models[37,69]. Although those experiments did not involve differential separation of the brain ECs from *bona fide* brain tissue and NC residing within brain ECs could contribute to measurements, both transmission electron microscopy and fluorescence microscopy visualized the presence of anti-ICAM-1 NCs crossing the BBB *in vivo* and further interacting with neurons[30,31]. At sites where anti-ICAM-1 NCs were observed to be in transit through brain ECs, cells junctions appeared to be intact and no blood-to-brain leakage of fluid-phase markers or radiolabeled albumin was measured[30]. Therefore, the cellular BBB model used here to measure transcytosis holds a good parallelism with *in vivo* data and can be used to study mechanistic aspects, otherwise difficult to examine in animal models.

Importantly, NPD altered NC transcytosis compared to inflammation, but not for all routes tested (figure 7 and supplementary figure S5). NPD increased the transcytosis rate for anti-ICAM-1 NC and anti-PV1 NCs, while it did not statistically alter that of anti-TfR NCs (supplementary figure S5a). Additionally, the absolute number of anti-ICAM-1 NC and anti-PV1 NCs transcytosed over 24 h decreased in NPD, while it did not change for anti-TfR NCs (supplementary figure S5b). Some of these data were unanticipated. For instance, the increased transcytosis rate for anti-ICAM-1 NCs was unexpected based on their decreased uptake rate described above, suggesting that possibly some fraction of NCs may be entrapped within brain ECs, perhaps in lysosomal compartments. This is possible since lysosomal trafficking of anti-ICAM-1 NCs in brain ECs has been reported[30] and NPD involves lysosomal changes[4,12,53]. Regarding anti-PV1 NCs, no change in their uptake rate or absolute endocytosis had been seen above, yet the same lysosomal entrapment paradigm would also apply to them, explaining a similar result. In contrast, the lack of change observed for anti-TfR NC transcytosis rate may indicate a different degree of lysosomal entrapment or perhaps, since PV1 and ICAM-1 associate with lipid rafts[51,78] that are altered in NPD[55–59], this may explain the result. Nevertheless, the absolute level of transcytosis for anti-ICAM-1 NCs surpassed that of the other two formulations in both the inflammation and NPD models.

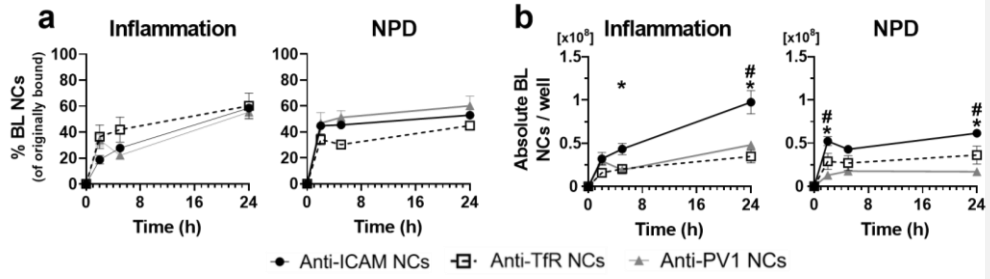

**Figure 7** Transcytosis of NCs targeted to three different transcytosis markers in inflammation or NPD. Brain ECs monolayers were treated with TNFα + imipramine (ASM deficiency) to simulate NPD, or with TNFα alone (inflammation) for an ASM-normal control. To assess transcytosis, $^{125}$I-antibody coated NCs targeted to either ICAM-1, TfR, or PV1 were added to the apical chamber for a 30-min binding pulse, washed to remove non-bound NCs, measured to obtain the NC cell-bound fraction, and cells were further incubated with NC-free medium for the indicated chase times. Then, the number of NCs in the basolateral (BL) fraction was assessed using a gamma counter. (a) NCs transcytosed to the BL chamber, expressed as the percentage of NCs originally bound to cells, to assess their transcytosis rate. (b) Total NCs in the BL fraction. Data are average ± SEM. *Compares anti-ICAM-1 NCs to anti-TfR NCs; #compares anti-ICAM-1 NCs to anti-PV1 NCs; no statistical significance was found between anti-TfR NCs and anti-PV1 NCs ($p < 0.05$ by one-way ANOVA).

### 3.4 Intracellular distribution of nanocarriers and disease effects in brain endothelial cells.

Transport involved in transcytosis employs membranous vesicles pinching off the endothelial plasma membrane by endocytic pathways[18]. In some instances, the resulting vesicles can also traffic to lysosomal compartments, as hypothesized above and empirically observed for some formulations[30,79], and found for some NCs targeted to receptors that lead to endocytic uptake but do not naturally associate with lysosomal transport[80]. Hence, the vesicular nature of these routes results in the membranous confinement of the cargo being transported across the BBB, which differs from p-glycoprotein-mediated mobilization of much smaller and membrane diffusible molecular cargo[81]. Confirming vesicular transport, under inflammation condition (TNFα), treatment of EC monolayers with amiloride to inhibit CAM-mediated endocytosis[33] significantly reduced uptake of anti-ICAM-1 NCs by brain ECs (supplementary Figure S6). Additionally, as speculated in section 3.3, under this condition, a fraction of internalized anti-ICAM-1 NCs trafficked to lysosomal compartments that had been labeled with Texas Red dextran: *e.g.* lysosomal colocalization at 24 h was 262.0 NCs/cell (Figure 8a,b). This observation is possible because when ECs are first incubated with dextran, this fluid phase marker can enter cells by any endocytic mechanism taking place and accumulate in Lamp-1-positive lysosomes, as previously shown[82]. Since mammalian lysosomes do not possess dextranases, dextran remains in this location for considerable time and, thus, it serves as a pH-independent lysosomal marker, contrarily to most common lysosomotropic agents which depend on the luminal pH of membranous vesicles[83]. Therefore, both sensitivity to an endocytic inhibitor and lysosomal colocalization support the vesicular nature of the transport of these NCs by brain ECs. Similarly, a fraction of anti-TfR NCs and anti-PV1 NCs also trafficked to lysosomes, i.e. in inflammation their 24 h lysosomal colocalization were 45.4 and 80.0 NCs/cell, respectively (figure 8a,b). Hence, just as transcytosis under this condition (Figure 7b), anti-ICAM-1 NCs surpassed both anti-TfR NCs and anti-PV1 NCs regarding lysosomal transport in brain ECs (Figure 8b), showing a parallelism with the original NC binding levels (Figure 4d) and supporting a receptor-mediated vesicular pathway.

NPD, mimicked by treating cells with TNFα + imipramine, decreased lysosomal colocalization of anti-ICAM-1 NCs, *e.g.* 155.8 NCs/cell at 24 h (supplemental figure S7a), which was similar to the lower lysosomal transport seen for anti-PV1 NC at most times, although not at 24 h (supplemental figure S7c) and different than anti-TfR NCs, which showed increased lysosomal transport by this time (84.2 lysosomal NCs/cell; supplemental figure S7b). This could explain the NPD-mediated increase in the transcytosis rate observed for anti-ICAM-1 NCs and anti-PV1 NCs, but not the unchanged transcytosis rate of anti-TfR NCs under this condition (supplementary figure S5), for which some other factor may

be influencing the overall transport of targeted NCs. For instance, cellular re-uptake of BL NCs to BL-to-AP transport could play a role. Regardless of these changes, the absolute number of anti-ICAM-1 NCs in EC lysosomes remained the highest under NPD condition (Figure 8c), just as they had remained the highest at transcytosis (figure 7b). This superiority regarding both intra-endothelial-lysosome and trans-endothelial transport of anti-ICAM-1 NCs is relevant because not only cells residing in the brain parenchyma, such as neurons and glial cells, but also brain ECs suffer from ASM deficiency in NPD patients[3,4]. Therefore, anti-ICAM-1 NCs may improve disease treatment by delivering adequate therapeutics (*e.g.* recombinant ASM) to both environments.

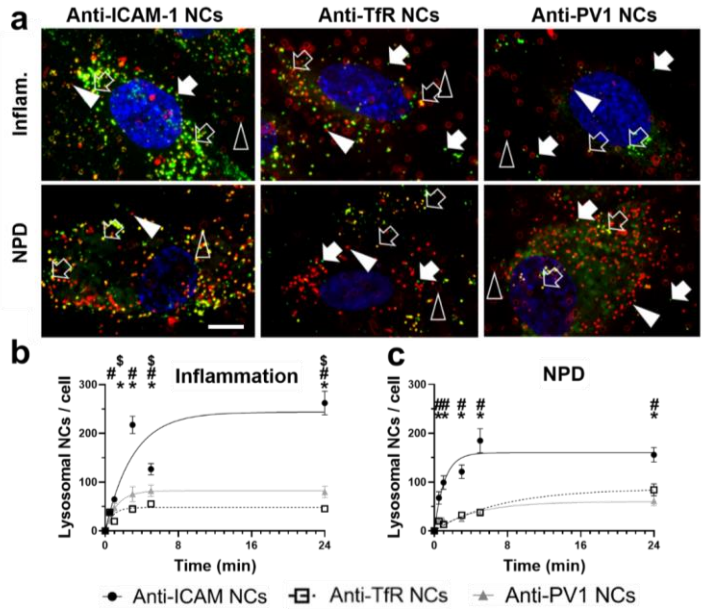


**Figure 8** NC transport to lysosomes in brain ECs. Brain ECs grown to confluency on transwells were treated with TNFα to mimic inflammation (ASM normal) or treated with both TNFα + imipramine to mimic NPD (ASM deficient). Then, cells were incubated for 40 min with Texas Red dextran (10 kDa) to allow its fluid-phase uptake, washed, and incubated in dextran-free cell medium for 1 h to allow internalized dextran to travel to lysosomes. Thereafter, cells were incubated for 30 min with green-fluorescent NCs, washed to remove non-bound NCs, and incubated with NC-free cell medium up to the indicated chases times. Cells were then fixed and nuclei were stained with DAPI. (a) This protocol reveals lysosomal colocalizing NCs in yellow (green + red; open arrows) from NCs at other locations (green; white arrows) and NC-empty lysosomes (red; white arrowheads) by fluorescence microscopy. Scale bar = 10 µm. (b,c) NCs colocalizing with dextran-labeled lysosomes in (b) inflammation and (c) NPD conditions. Data are average ± SEM. *Compares anti-ICAM-1 NCs to anti-TfR NCs; #compares anti-ICAM-1 NCs to anti-PV1 NCs; $compares anti-TfR NCs to anti-PV1 NCs ($p < 0.05$ by one-way ANOVA).

### 3.5 Basolateral re-uptake of anti-ICAM-1 NCs and disease effects.

The avidity with which a targeted formulation binds to their receptors on brain ECs had been shown to impact transcytosis[30,79,84]. Particularly for anti-ICAM-1 NCs, our previous study compared three different Ab coatings on the NC surface, where the formulations with highest and lowest Ab molecules per NC transcytosed worse than those with intermediate Ab levels[30]. This was due to the fact that low Ab coating lowered apical binding and uptake, while highly coated NCs did not detach well from ICAM-1 at the BL side of cells after transcytosis[30]. Therefore, it is possible that transcytosed anti-ICAM-1 NCs still attached to cells or accumulating between their BL membrane and the transwell filter are re-internalized by cells. Then, this additional event would impact the final level of transcytosis measured at the BL chamber below the transwell filter.

To discern this, brain EC monolayers were incubated with green-fluorescent anti-ICAM-1 NCs added to the apical side for 30 min to allow for binding, then washed to remove non-bound NCs. Next, while pre-bound NCs were allowed to transcytose, red-fluorescent dextran was added to the BL chamber (supplementary figure S8a), which did not cross the cellular monolayer to reach the AP side (supplementary figure S8b). Hence, if NCs transcytosed to the BL side of cells were re-internalized by them, fluid-phase dextran would enter these vesicles and co-localize with NCs (green + red = yellow, figure 9a). In fact, 39.8% of NCs at the cell fraction colocalized with dextran, as visualized by fluorescence microscopy, demonstrating anti-ICAM-1 NC reuptake after transcytosis. As a control, only 8% colocalization was seen when dextran was added to the BL chamber and then removed before NCs were added to the AP side (figure 9a).

After verifying BL re-uptake, the rate of BL endocytosis was independently evaluated by adding NCs at the BL side (figure 9b) and using the dextran-free fluorescence microscopy method described for AP uptake in figure 5. The rate of BL endocytosis of anti-ICAM-1 NCs was lower in NPD compared to inflammation, *e.g.* 64% *vs.* 83% internalization at 3 h, respectively (figure 9b). Decreased rate for BL uptake of anti-ICAM-1 NCs in NPD pairs well with their increased transcytosis rate because these are competing events. Also, this decreased rate for BL uptake in NPD agrees with the decreased rate of AP uptake seen above (figure 5). As described[78], ASM-mediated ceramide formation supports CAM-mediated endocytosis and, thus, it was expected that ASM deficiency in NPD would alter BL uptake similarly.

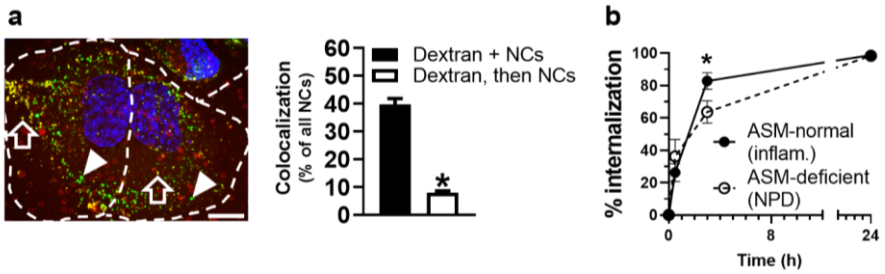


**Figure 9** Basolateral reuptake of anti-ICAM-1 NCs by ECs and NPD effect. (a) TNFα-activated brain EC monolayers (inflammation) were incubated with green-fluorescent anti-ICAM-1 NCs added to the apical chamber for a 30-min binding pulse, washed to remove non-bound NCs, and further incubated for 30 min with NC-free medium. At this time, Texas Red dextran was added as a fluid phase marker to the basolateral chamber, so that if cells re-internalize NCs transcytosed to the basolateral side, the fluid phase entering these vesicles could be traced and colocalized with green NCs, appearing as yellow (green+red; arrows) *vs.* NCs inside cells from the apical side (green alone; arrowheads). Samples were visualized and quantified by fluorescence microscopy, of which a representative confocal image is shown (NCs, then dextran). Blue = cell nuclei. Scale bar = 10 μm. A control experiment with dextran added prior to NC incubation was also quantified (dextran, then NCs). (b) Basolateral uptake of anti-ICAM-1 NCs was tested in cells treated with TNFα + imipramine to mimic ASM-deficient NPD *vs.* cell treated with TNFα alone as an inflammation, ASM-normal comparison. Cells were incubated for a 30-min binding pulse with green-fluorescent NCs, washed, fixed, incubated in NC-free medium to allow uptake, fixed, and counterstained with red-secondary Ab to distinguish intracellular (green only) NCs from cell-bound (green + red = yellow) NCs by fluorescence microscopy. Data are average ± SEM. *$p<0.05$ by Student's t-test.

## 4 CONCLUSION

In summary (figure 10), in inflammation, ICAM-1 was more highly expressed compared to TfR and much more than PV1. ASM deficiency markedly, modestly, and slightly increased the expression of ICAM-1, PV1, and TfR, respectively. Hence, in this cellular model involving both, enzyme deficiency and inflammation, ICAM-1 was much highly expressed than the other markers, explaining much higher NC binding. ASM deficiency decreased the uptake rate for anti-ICAM-1 NCs, expected since this enzyme is involved in the CAM pathway[78], without affecting that of the other formulations. Yet, due to its much higher NC binding, the absolute level of internalized anti-ICAM-1 NCs still surpassed the other two formulations. Curiously, ASM deficiency increased the transcytosis rate for both anti-ICAM-1 NCs and anti-PV1 NCs, leaving anti-TfR NCs transcytosis rate unaffected. This could be explained in part by the fact that ASM deficiency decreased competing lysosomal transport of anti-ICAM NCs and anti-PV1 NCs, although the increased lysosomal transport of anti-TfR NCs does not pair well with their unchanged transcytosis in NPD. Nevertheless, due to the originally lower level of binding and uptake of anti-PV1 NCs compared to anti-TfR NCs, the absolute transcytosis of these formulations was rather similar in NPD, while that of anti-ICAM-1 NCs remained highest. Interestingly, increased transcytosis rates in NPD for anti-ICAM-1 NCs and anti-PV1 NCs would be expected to increase the absolute number of NCs being transcytosed, but this value decreased for both formulations. While there is no current explanation for these phenomena, perhaps other competing mechanisms could take place, such as BL re-uptake of NCs. In fact, this was verified for anti-ICAM-1 NCs, which were observed to undergo re-uptake at the BL side of cells following transcytosis. Just as ASM deficiency

had lowered AP uptake rate for this formulation, it had also decreased their BL uptake rate, hence, leading to higher transcytosis rate. In conclusion, ASM deficiency had different effects on the brain EC interaction of anti-ICAM-1 NCs, anti-TfR NCs, and anti-PV1 NCs, where the former formulation offered the overall most favorable results due to the highest number of transcytosed NCs, thus representing a promising strategy to deliver therapeutics across the BBB for neuronopathic NPD.

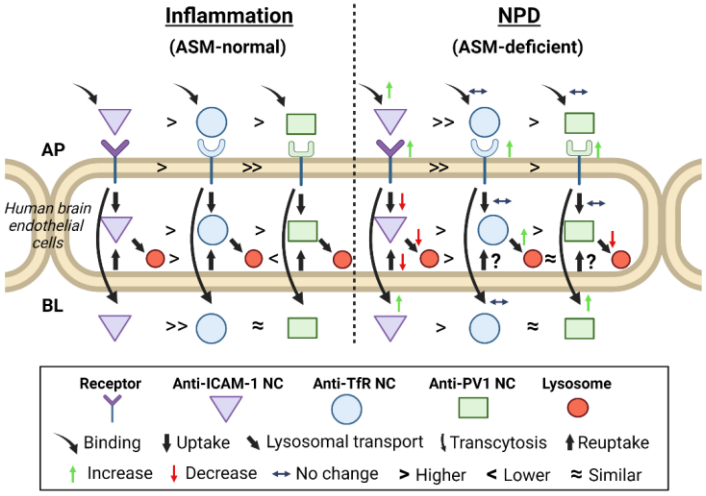


**Figure 10** Schematic representation of NPD effects on brain EC interactions with targeted NCs. The cartoon summarizes the effects of NPD, encompassing both inflammation and ASM deficiency compared to inflammation alone as an ASM-normal control, on the marker expression and NC transport *via* ICAM-1, TfR, and PV1 in BBB models. Changes in rates are indicated relative to NC binding, uptake, re-uptake and overall transcytosis as green arrows (increased), red arrows (decreased), or blue arrows (unchanged). Relative absolute levels of NCs bound to cells, within cell, within lysosomes, or crossing cells are indicated as > (higher than), < (lower than), and ≈ (similar than). AP = apical; BL = basolateral.

## 5 ETHICAL STATEMENT

5.1 **Ethics approval and consent to participate.** This study did not involve human subjects. The human cell model used is a commercial cell line with no personal information.

5.2 **Consent for publication.** All authors have read and approved this manuscript.

5.3 **Availability of data and materials.** Data will be provided upon request. Unique materials can be shared upon reasonable request and at recipient cost, respecting protection of any active confidentiality and intellectual property provisions.

5.4 **Competing interests.** Authors declare no conflict of interest.

5.5 **Funding.** SM: RTI2018-101034-B-I00 from the Spanish Ministry of Science and Innovation (MCIN/AEI/ 10.13039/501100011033) and "ERDF A way of making Europe", and CERCA Program (Generalitat de Catalunya). ML: INPhINIT Predoctoral Fellowship (LCF/BQ/DI18/11660018) funded by Fundación La Caixa and Horizon 2020 Marie Sklodowska-Curie (grant 713673). MP: FPI PRE2021-098133 funded by the Spanish Ministry of Science and Innovation (MCIN/AEI/ 10.13039/501100011033) and "ESF Investing in your future".

**5.6 Authors' contributions.** M.L. performed and analyzed majority of the experiments, drafted the manuscript, and prepared figures. M.P. performed and analyzed the flow cytometry experiment, prepared respective figure, and helped edit the manuscript. S.M conceptualized and directed the investigation, secured funding, helped plan experiments and interpret results, and helped write and edit the text and figures.

**5.7 Acknowledgements.** BioRender.com was used for the creation of the graphical abstract and figure 10.

## 6 REFERENCES

1. OMIM Entry - # 257200 - NIEMANN-PICK DISEASE, TYPE A.
2. OMIM Entry - # 607616 - NIEMANN-PICK DISEASE, TYPE B.
3. Vanier, M. T. Niemann–Pick diseases. *Handb. Clin. Neurol.* **113**, 1717–1721 (2013).
4. Schuchman, E. H. The pathogenesis and treatment of acid sphingomyelinase-deficient Niemann-Pick disease. *J. Inherit. Metab. Dis.* **30**, 654–663 (2007).
5. Quinn, P. J. Sphingolipid symmetry governs membrane lipid raft structure. *Biochim. Biophys. Acta* **1838**, 1922–1930 (2014).
6. Abe, A. & Shayman, J. A. Sphingolipid Catabolism. *Encycl. Biol. Chem. Second Ed.* 287–292 (2013)
7. Breiden, B. & Sandhoff, K. Acid Sphingomyelinase, a Lysosomal and Secretory Phospholipase C, Is Key for Cellular Phospholipid Catabolism. *Int. J. Mol. Sci. 2021, Vol. 22, Page 9001* **22**, 9001 (2021).
8. Wasserstein, M. P. *et al.* The natural history of type B Niemann-Pick disease: results from a 10-year longitudinal study. *Pediatrics* **114**, e672-677 (2004).
9. Hollak, C. E. M. *et al.* Acid sphingomyelinase (Asm) deficiency patients in The Netherlands and Belgium: disease spectrum and natural course in attenuated patients. *Mol. Genet. Metab.* **107**, 526–533 (2012).
10. McGovern, M. M. *et al.* A prospective, cross-sectional survey study of the natural history of Niemann-Pick disease type B. *Pediatrics* **122**, e341-349 (2008).
11. Marín, T. *et al.* c-Abl Activation Linked to Autophagy-Lysosomal Dysfunction Contributes to

Neurological Impairment in Niemann-Pick Type A Disease. *Front. cell Dev. Biol.* **10**, 1482-1499 (2022).

12. Carsana, E. V. *et al.* Massive Accumulation of Sphingomyelin Affects the Lysosomal and Mitochondria Compartments and Promotes Apoptosis in Niemann-Pick Disease Type A. *J. Mol. Neurosci.* **72**, 1482–1499 (2022).

13. Gabandé-Rodríguez, E. *et al.* Lipid-induced lysosomal damage after demyelination corrupts microglia protective function in lysosomal storage disorders. *EMBO J.* **38**, e99553 (2019).

14. McGovern, M. M., Aron, A., Brodie, S. E., Desnick, R. J. & Wasserstein, M. P. Natural history of Type A Niemann-Pick disease: possible endpoints for therapeutic trials. *Neurology* **66**, 228–232 (2006).

15. Keam, S. J. Olipudase Alfa: First Approval. *Drugs* **82**, 941–947 (2022).

16. He, X. *et al.* Characterization of human acid sphingomyelinase purified from the media of overexpressing Chinese hamster ovary cells. *Biochim. Biophys. Acta* **1432**, 251–264 (1999).

17. Diaz, G. A. *et al.* One-year results of a clinical trial of olipudase alfa enzyme replacement therapy in pediatric patients with acid sphingomyelinase deficiency. *Genet. Med.* **23**, 1543–1550 (2021).

18. Muro, S. Strategies for delivery of therapeutics into the central nervous system for treatment of lysosomal storage disorders. *Drug Deliv. Transl. Res.* **2**, 169–186 (2012).

19. Miranda, S. R. P. *et al.* Infusion of recombinant human acid sphingomyelinase into niemann-pick disease mice leads to visceral, but not neurological, correction of the pathophysiology. *FASEB J.* **14**, 1988–1995 (2000).

20. Tomsen-Melero, J. *et al.* Liposomal formulations for treating lysosomal storage disorders. *Adv. Drug Deliv. Rev.* **190**, 114531 (2022).

21. Solomon, M. & Muro, S. Lysosomal enzyme replacement therapies: Historical development, clinical outcomes, and future perspectives. *Adv. Drug Deliv. Rev.* **118**, 109–134 (2017).

22. Del Grosso, A., Parlanti, G., Mezzena, R. & Cecchini, M. Current treatment options and novel nanotechnology-driven enzyme replacement strategies for lysosomal storage disorders. *Adv. Drug Deliv. Rev.* **188**, 114464 (2022).

23. Seras-Franzoso, J. *et al.* Extracellular vesicles from recombinant cell factories improve the activity and efficacy of enzymes defective in lysosomal storage disorders. *J. Extracell. Vesicles* **10**, e12058 (2021).

24. Schuster, T. *et al.* Potential of surfactant-coated nanoparticles to improve brain delivery of arylsulfatase A. *J. Control. Release* **253**, 1–10 (2017).

25. Mayer, F. Q. *et al.* Laronidase-functionalized multiple-wall lipid-core nanocapsules: promising formulation for a more effective treatment of mucopolysaccharidosis type I. *Pharm. Res.* **32**, 941–954 (2015).

26. Salvalaio, M. *et al.* Targeted polymeric nanoparticles for brain delivery of high molecular weight molecules in lysosomal storage disorders. *PLoS One* **11**, 1–17 (2016).

27. Rigon, L. *et al.* Targeting brain disease in MPSII: Preclinical evaluation of IDS-loaded PLGA nanoparticles. *Int. J. Mol. Sci.* **20**, 1–15 (2019).

28. Grosso, A. Del *et al.* Brain-targeted enzyme-loaded nanoparticles: A breach through the blood-brain barrier for enzyme replacement therapy in Krabbe disease. *Sci. Adv.* **5**, eaax7462 (2019).

29. Tian, X. *et al.* LRP-1-mediated intracellular antibody delivery to the Central Nervous System. *Sci. Rep.* **5**, 11990 (2015).

30. Manthe, R. L. *et al.* Intertwined mechanisms define transport of anti-ICAM nanocarriers across the endothelium and brain delivery of a therapeutic enzyme. *J. Control. Release* **324**, 181–193 (2020).

31. Muntimadugu, E. *et al.* Comparison between Nanoparticle Encapsulation and Surface Loading for Lysosomal Enzyme Replacement Therapy. *Int. J. Mol. Sci.* **23**, 4034 (2022).

32. Muro, S. Intercellular adhesion molecule-1 and vascular cell adhesion molecule-1. in *Endothelial biomedicine* (ed. Aird, W.) 1058–1070 (Cambridge University Press, 2007).

33. Muro, S. *et al.* A novel endocytic pathway induced by clustering endothelial ICAM-1 or PECAM-1. *J. Cell Sci.* **116**, 1599–609 (2003).

34. Muro, S., Schuchman, E. H. & Muzykantov, V. R. Lysosomal enzyme delivery by ICAM-1-targeted nanocarriers bypassing glycosylation- and clathrin-dependent endocytosis. *Mol. Ther.* **13**, 135–141 (2006).

35. Garnacho, C. & Muro, S. ICAM-1 targeting, intracellular trafficking, and functional activity of polymer nanocarriers coated with a fibrinogen-derived peptide for lysosomal enzyme replacement. *J. Drug Target.* **25**, 786–795 (2017).

36. Garnacho, C., Dhami, R., Solomon, M., Schuchman, E. H. & Muro, S. Enhanced Delivery and Effects of Acid Sphingomyelinase by ICAM-1-Targeted Nanocarriers in Type B Niemann-Pick Disease Mice. *Mol. Ther.* **25**, 1686–1696 (2017).

37. Papademetriou, J. *et al.* Comparative binding, endocytosis, and biodistribution of antibodies and antibody-coated carriers for targeted delivery of lysosomal enzymes to ICAM-1 versus transferrin receptor. *J. Inherit. Metab. Dis.* **36**, 467–77 (2013).

38. Garnacho, C. *et al.* Delivery of acid sphingomyelinase in normal and niemann-pick disease mice using intercellular adhesion molecule-1-targeted polymer nanocarriers. *J. Pharmacol. Exp. Ther.* **325**, 400–408 (2008).

39. Muro, S. *et al.* Control of endothelial targeting and intracellular delivery of therapeutic enzymes by modulating the size and shape of ICAM-1-targeted carriers. *Mol. Ther.* **16**, 1450–1458 (2008).

40. Papademetriou, I. T., Garnacho, C., Schuchman, E. H. & Muro, S. In vivo performance of

polymer nanocarriers dually-targeted to epitopes of the same or different receptors. *Biomaterials* **34**, 3459–66 (2013).

41. Hsu, J., Rappaport, J. & Muro, S. Specific binding, uptake, and transport of ICAM-1-targeted nanocarriers across endothelial and subendothelial cell components of the blood-brain barrier. *Pharm. Res.* **31**, 1855–66 (2014).

42. Marcos-Contreras, O. A. *et al.* Combining vascular targeting and the local first pass provides 100-fold higher uptake of ICAM-1-targeted vs untargeted nanocarriers in the inflamed brain. *J. Control. Release* **301**, 54–61 (2019).

43. Glassman, P. M. *et al.* Targeted nanocarriers coopting pulmonary leukocytes for drug delivery to the injured brain. *bioRxiv* 479150 (2022).

44. Moos, T., Nielsen, T. R., Skjørringe, T. & Morgan, E. H. Iron trafficking inside the brain. *J. Neurochem.* **103**, 1730–1740 (2007).

45. Pardridge, W. M. Blood–brain barrier delivery. *Drug Discov. Today* **12**, 54–61 (2007).

46. Pardridge, W. M. Blood-brain barrier delivery for lysosomal storage disorders with IgG-lysosomal enzyme fusion proteins. *Adv. Drug Deliv. Rev.* **184**, 114234 (2022).

47. Wu, L. & Gonias, S. L. The low-density lipoprotein receptor-related protein-1 associates transiently with lipid rafts. *J. Cell. Biochem.* **96**, 1021–1033 (2005).

48. Taylor, D. R. & Hooper, N. M. The low-density lipoprotein receptor-related protein 1 (LRP1) mediates the endocytosis of the cellular prion protein. *Biochem. J.* **402**, 17–23 (2007).

49. Schnitzer, J. E. Caveolae: from basic trafficking mechanisms to targeting transcytosis for tissue-specific drug and gene delivery in vivo. *Adv. Drug Deliv. Rev.* **49**, 265–80 (2001).

50. Tosi, G. *et al.* Investigation on mechanisms of glycopeptide nanoparticles for drug delivery across the blood-brain barrier. *Nanomedicine (Lond).* **6**, 423–436 (2011).

51. Stan, R. V. *et al.* The diaphragms of fenestrated endothelia – gatekeepers of vascular permeability and blood composition. *Dev. Cell* **23**, 1203 (2012).

52. Shuvaev, V. V. *et al.* Targeting superoxide dismutase to endothelial caveolae profoundly alleviates inflammation caused by endotoxin. *J. Control. Release* **272**, 1–8 (2018).

53. Schuchman, E. H. & Desnick, R. J. Types A and B Niemann-Pick Disease. *Mol. Genet. Metab.* **120**, 27 (2017).

54. Gabandé-Rodríguez, E., Boya, P., Labrador, V., Dotti, C. G. & Ledesma, M. D. High sphingomyelin levels induce lysosomal damage and autophagy dysfunction in Niemann Pick disease type A. *Cell Death Differ.* **21**, 864–875 (2014).

55. Breiden, B. & Sandhoff, K. Mechanism of Secondary Ganglioside and Lipid Accumulation in Lysosomal Disease. *Int. J. Mol. Sci.* **21**, (2020).

56. Breilyn, M. S., Zhang, W., Yu, C. & Wasserstein, M. P. Plasma lyso-sphingomyelin levels are positively associated with clinical severity in acid sphingomyelinase deficiency. *Mol. Genet. Metab. Reports* **28**, 100780 (2021).

57. Van Meer, G., Voelker, D. R. & Feigenson, G. W. Membrane lipids: where they are and how they behave. *Nat. Rev. Mol. Cell Biol. 2008 92* **9**, 112–124 (2008).

58. Stieger, B., Steiger, J. & Locher, K. P. Membrane lipids and transporter function. *Biochim. Biophys. Acta - Mol. Basis Dis.* **1867**, 166079 (2021).

59. Casares, D., Escribá, P. V. & Rosselló, C. A. Membrane Lipid Composition: Effect on Membrane and Organelle Structure, Function and Compartmentalization and Therapeutic Avenues. *Int. J. Mol. Sci.* **20**, 2167 (2019).

60. Simons, K. & Gruenberg, J. Jamming the endosomal system: lipid rafts and lysosomal storage diseases. *Trends Cell Biol.* **10**, 459–462 (2000).

61. Fraldi, A. *et al.* Lysosomal fusion and SNARE function are impaired by cholesterol accumulation in lysosomal storage disorders. *EMBO J.* **29**, 3607 (2010).

62. Rappaport, J., Garnacho, C. & Muro, S. Clathrin-mediated endocytosis is impaired in type A-B Niemann-Pick disease model cells and can be restored by ICAM-1-mediated enzyme replacement. *Mol. Pharm.* **11**, 2887–2895 (2014).

63. Rappaport, J., Manthe, R. L., Solomon, M., Garnacho, C. & Muro, S. A Comparative Study on the Alterations of Endocytic Pathways in Multiple Lysosomal Storage Disorders. *Mol. Pharm.* **13**, 357–368 (2016).

64. Dhami, R. & Schuchman, E. H. Mannose 6-phosphate receptor-mediated uptake is defective in acid sphingomyelinase-deficient macrophages: implications for Niemann-Pick disease enzyme replacement therapy. *J. Biol. Chem.* **279**, 1526–1532 (2004).

65. Rappaport, J., Manthe, R. L., Garnacho, C. & Muro, S. Altered clathrin-independent endocytosis in type A Niemann-Pick disease cells and rescue by ICAM-1-targeted enzyme delivery. *Mol. Pharm.* **12**, 1366–1376 (2015).

66. Roki, N. *et al.* A method to improve quantitative radiotracing-based analysis of the in vivo biodistribution of drug carriers. *Bioeng. Transl. Med.* **6**, e10298 (2021).

67. Wiseman, M. E. & Frank, C. W. Antibody adsorption and orientation on hydrophobic surfaces. *Langmuir* **28**, 1765–1774 (2012).

68. Beckmann, N., Sharma, D., Gulbins, E., Becker, K. A. & Edelmann, B. Inhibition of acid sphingomyelinase by tricyclic antidepressants and analogons. *Front. Physiol.* **5**, 331 (2014).

69. Solomon, M. *et al.* Altered blood-brain barrier transport of nanotherapeutics in lysosomal storage diseases. *J. Control. Release* **349**, 1031–1044 (2022).

70. Muro, S., Muzykantov, V. R. & Murciano, J. C. Characterization of endothelial internalization and targeting of antibody-enzyme conjugates in cell cultures and in laboratory animals.

*Methods Mol. Biol.* **283**, 21–36 (2004).

71. Bui, T. M., Wiesolek, H. L. & Sumagin, R. ICAM-1: A master regulator of cellular responses in inflammation, injury resolution, and tumorigenesis. *J. Leukoc. Biol.* **108**, 787–799 (2020).

72. Muro, S. *et al.* Endothelial targeting of high-affinity multivalent polymer nanocarriers directed to intercellular adhesion molecule 1. *J. Pharmacol. Exp. Ther.* **317**, 1161–1169 (2006).

73. Schuchman, E. H. Acid sphingomyelinase, cell membranes and human disease: lessons from Niemann-Pick disease. *FEBS Lett.* **584**, 1895–1900 (2010).

74. Brenner, J. S. *et al.* Mechanisms that determine nanocarrier targeting to healthy versus inflamed lung regions. *Nanomedicine* **13**, 1495–1506 (2017).

75. Myerson, J. W. *et al.* Flexible Nanoparticles Reach Sterically Obscured Endothelial Targets Inaccessible to Rigid Nanoparticles. *Adv. Mater.* **30**, 1802373 (2018).

76. Myerson, J. W. *et al.* Non-affinity factors modulating vascular targeting of nano- and microcarriers. *Adv. Drug Deliv. Rev.* **99**, 97–112 (2016).

77. Hsu, J., Hoenicka, J. & Muro, S. Targeting, endocytosis, and lysosomal delivery of active enzymes to model human neurons by ICAM-1-targeted nanocarriers. *Pharm. Res.* **32**, 1264–78 (2015).

78. Serrano, D., Bhowmick, T., Chadha, R., Garnacho, C. & Muro, S. Intercellular adhesion molecule 1 engagement modulates sphingomyelinase and ceramide, supporting uptake of drug carriers by the vascular endothelium. *Arterioscler. Thromb. Vasc. Biol.* **32**, 1178–85 (2012).

79. Yu, Y. J. *et al.* Boosting brain uptake of a therapeutic antibody by reducing its affinity for a transcytosis target. *Sci. Transl. Med.* **3**, 84ra44 (2011).

80. Daniele, R. *et al.* Influence of Folate-Targeted Gold Nanoparticles on Subcellular Localization and Distribution into Lysosomes. *Pharmaceutics* **15**, 864 (2023).

81. Prachayasittikul, V., Worachartcheewan, A., Shoombuatong, W., Prachayasittikul, V. & Nantasenamat, C. CLASSIFICATION OF P-GLYCOPROTEIN-INTERACTING COMPOUNDS USING MACHINE LEARNING METHODS. *EXCLI J.* **14**, 958–970 (2015).

82. Muro, S. *et al.* Slow intracellular trafficking of catalase nanoparticles targeted to ICAM-1 protects endothelial cells from oxidative stress. *Am. J. Physiol. Physiol.* **285**, C1339–C1347 (2003).

83. Johnson, D. E., Ostrowski, P., Jaumouillé, V. & Grinstein, S. The position of lysosomes within the cell determines their luminal pH. *J. Cell Biol.* **212**, 692 (2016).

84. Bien-Ly, N. *et al.* Transferrin receptor (TfR) trafficking determines brain uptake of TfR antibody affinity variants. *J. Exp. Med.* **211**, 233–244 (2014).

**Supplemental information:**

# Effect of Acid Sphingomyelinase Deficiency in Type A Niemann-Pick Disease on the Transport of Therapeutic Nanocarriers Across the Blood-Brain Barrier

**Maximilian Loeck[1], Marina Placci[1], and Silvia Muro[1,2]**

[1]Institute for Bioengineering of Catalonia of the Barcelona Institute of Science and Technology, Barcelona, Spain

[2]Institution of Catalonia for Research and Advanced Studies, Barcelona, Spain

*** Correspondence:** Silvia Muro; smuro@ibecbarcelona.eu

**Keywords:** drug nanocarriers, blood-brain barrier, receptor-mediated transcytosis, ICAM-1, transferrin receptor, PV-1, lysosomal storage disease, ASM deficiency, Niemann-Pick disease type A.

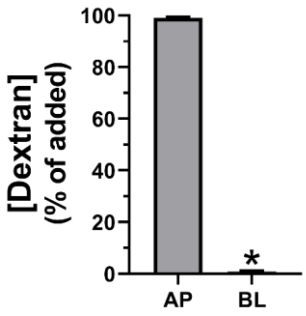


**Figure S1 Lack of dextran leakage through brain EC monolayers. TNFα-treated brain EC monolayers grown for 7 days to confluency on transwell filters were incubated for 30 min with Texas Red dextran (10 kDa) added to the apical (AP) chamber. Then, dextran was measured at both the AP and basolateral (BL) chambers by spectrofluorometry, from which dextran concentration in either chamber was calculated. Results are expressed as a percent of the originally added concentration. Data are average ± SEM. *Compares BL vs. AP ($p < 0.05$ by Student's t-test).**

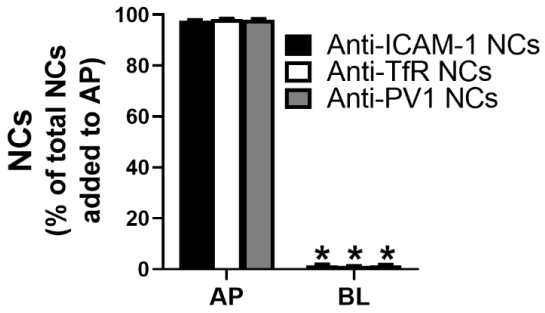


**Figure S2** Lack of NC leakage through brain EC monolayers. TNFα-treated brain EC monolayers grown for 7 days to confluency on transwell filters were incubated for 30 min with $^{125}$I-antibody coated NCs targeted to either ICAM-1, TfR, or PV1, which were added to the AP chamber over the EC monolayer and then measured in both chambers using a gamma counter. Results were calculated as a percent of the originally added concentration. Data are average ± SEM. *Compares BL *vs*. AP ($p < 0.05$ by Student's t-test).

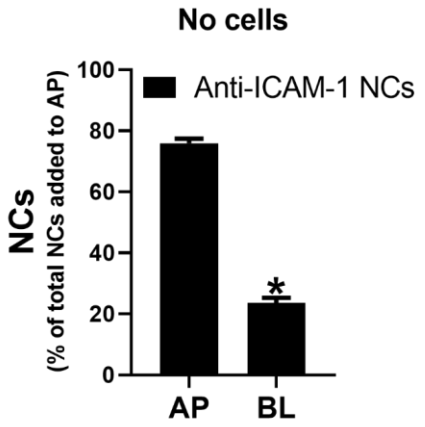


**Figure S3** Permeability of transwell filters to Ab-coated NCs. $^{125}$I-antibody coated NCs targeted to ICAM-1 were added to the AP chamber over transwell filters voided of cells. After 30 min, NCs were measured in both chambers using a gamma counter. Results were calculated as a percent of the originally added concentration. Data are average ± SEM. *Compares BL *vs*. AP ($p < 0.05$ by Student's t-test).

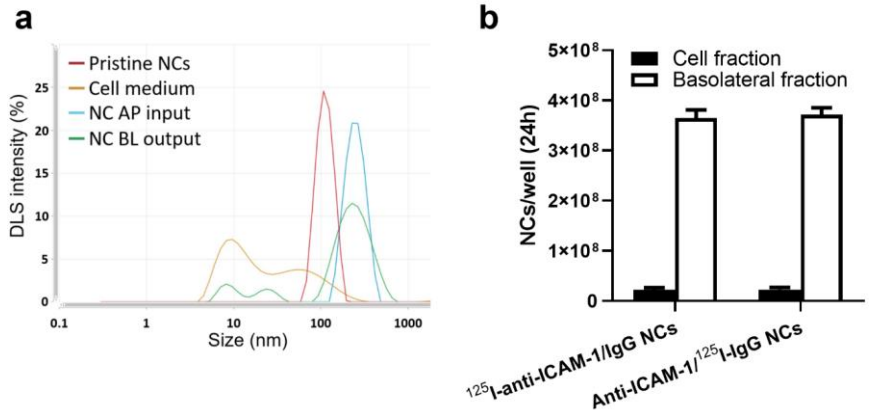


**Figure S4 Integrity of targeted NCs during cellular experiments. (a) Dynamic light scattering measurement of the hydrodynamic diameter of pristine uncoated NCs and NCs coated with anti-ICAM-1 prior to adding them (input) to the apical (AP) chamber over TNFα-treated EC monolayers and after (output) 30 min transcytosis into the basolateral (BL) chamber. (b) Comparison of the cellular fraction and BL fraction of targeted NCs incubated with cells for a 30 min binding pulse, then measured after 24 h transport chase, where formulations had been coated with a 1:1 molar ratio $^{125}$I-anti-ICAM-1:IgG or anti-ICAM-1:$^{125}$I-IgG. Data are average ± SEM. No significance was found between formulations ($p > 0.05$ by Student's t-test).**

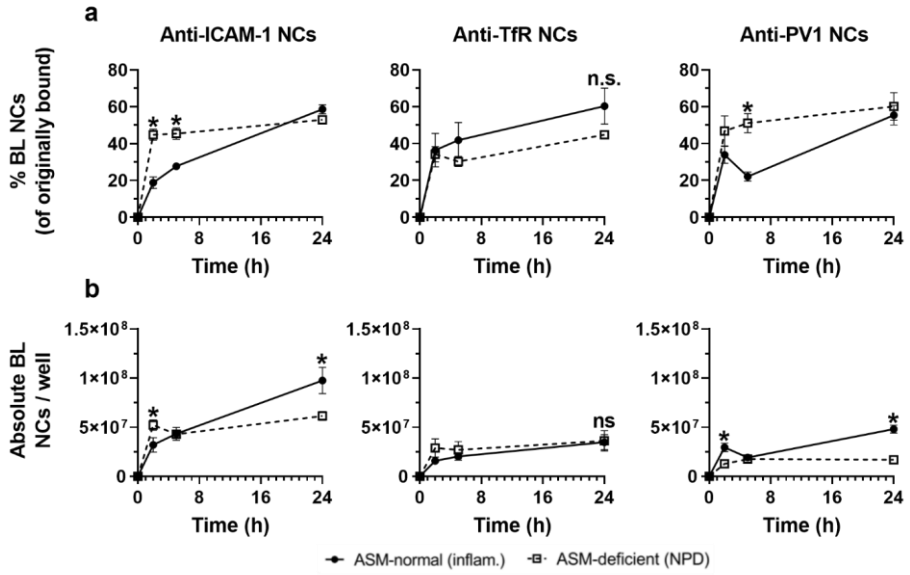


**Figure S5 Effect of ASM deficiency on NC transcytosis across EC monolayers. Brain ECs monolayers were treated with TNF*α* and imipramine (ASM deficiency) to simulate NPD, or with TNF*α* alone (inflammation) for an ASM-normal control. To assess transcytosis, $^{125}$I-labelled NCs targeted to either ICAM-1, TfR, or PV1 were added to the apical chamber for a 30-min binding pulse, washed to remove non-bound NCs, measured to obtain the NC bound fraction, and cells were further incubated with NC-free medium for the indicated chase times. Then, the number of NCs in the basolateral (BL) fraction was assessed using a gamma counter. (a) NCs transcytosed to the BL chamber, expressed as the percentage of NCs originally bound to cells, to assess their transcytosis rate. (b) Total NCs in the BL fraction. Data are average ± SEM. $p<0.05$ by Student's t test, *compares ASM-deficient NPD to ASM-normal inflammation condition.**

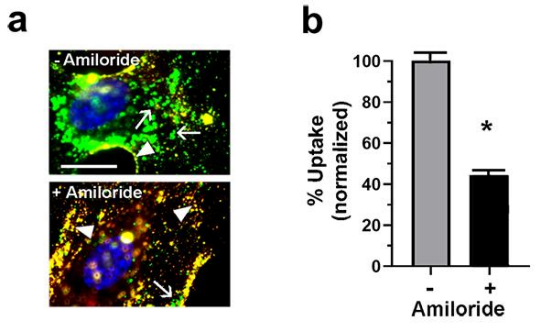


**Figure S6 Anti-ICAM-1 NCs uptake mechanism by brain ECs. Brain ECs monolayers treated with TNFα were incubated for 3 h with green-fluorescent anti-ICAM-1 NCs in either control cell medium or medium containing amiloride, which is known to inhibit CAM-mediated endocytosis. Cells were then washed, fixed, and NCs bound on the cell surface were counterstained with red-fluorescent secondary antibody to distinguish internalized NCs (green, arrows) from surface-bound NCs (green + red = yellow, arrowheads). Samples were (a) imaged and (b) quantified by fluorescence microscopy to calculate percent internalization as in figure 5. (a) Blue = nuclei stained with DAPI; dashed lines = cell borders. Scale bar = 10 µm. (b) Data are average ± SEM, normalized to control (- amiloride). *Compares amiloride vs. control ($p<0.05$ by Student's t-test).**

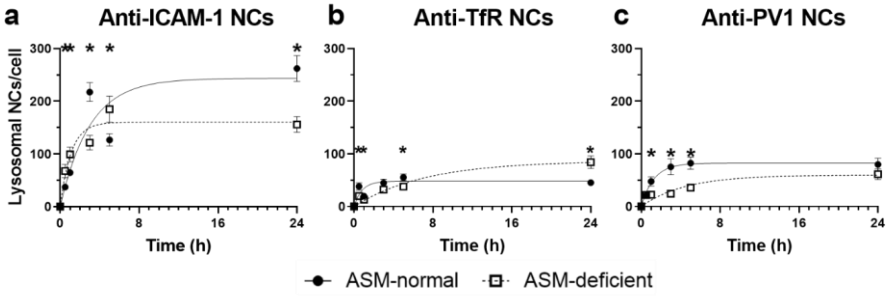


**Figure S7 Effect of ASM deficiency on lysosomal transport of NCs in brain ECs. Brain ECs monolayers were treated with TNFα and imipramine (ASM deficiency) to simulate NPD, or with TNFα alone (inflammation) for an ASM-normal condition. Cells were first incubated for 40 min with Texas Red dextran (10 kDa) to allow its fluid-phase uptake, then washed to remove non-internalized dextran, and further incubated for 1 h in dextran-free cell medium to enable internalized dextran to traffic to lysosomes, staining them red. Next, green-fluorescent NCs targeted to either (a) ICAM-1, (b) TfR, or (c) PV1 were added to the apical chamber for a 30-min binding pulse, washed to remove non-bound NCs, and cells were further incubated with NC-free cell medium for the indicated chase times, fixed, and analyzed by fluorescence microscopy to quantify the numbers of NCs colocalizing with dextran-labelled lysosomes. Data are average ± SEM. *Compares NPD (ASM deficient = TNFα + imipramine) vs. inflammation (ASM normal = TNFα) by Student's t-test (p<0.05).**

**Comentado [SM1]:** -It should be a,b,c instead of A,B,C
-It should ne NCs instead of NC
-Delete all % data and place a,b,c horizontal as in old S5
-The key ASM normal deficient should be as in old S5

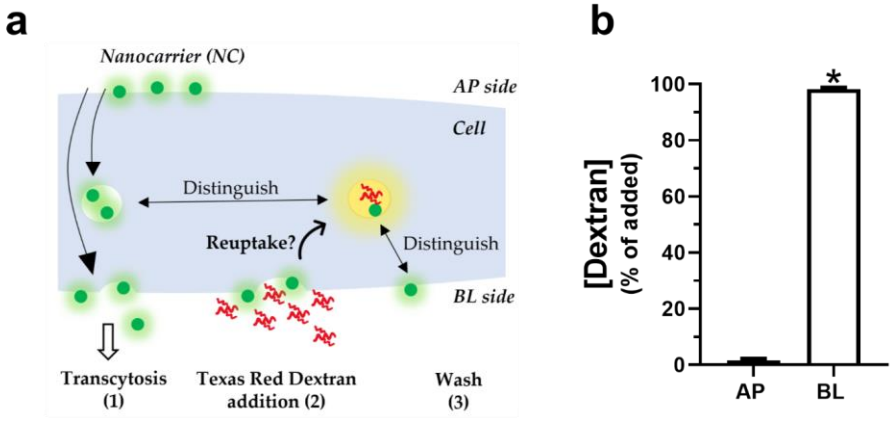


**Figure S8 Schematic of the method used to visualize basolateral reuptake of anti-ICAM-1 nanocarriers (NCs) by endothelial cell monolayers. (a) Cells were incubated for 30 min with green-fluorescent NCs added to the apical (AP) side to allow for binding, followed by washing to remove non-bound NCs. To distinguish NCs in basolateral (BL) reuptake vesicles from all NCs not in reuptake, cells were then incubated for 30 min with NC-free medium added to the AP side, and NC-free medium containing the fluid phase marker Texas Red dextran added to the BL side. Ultimately, cells were washed to remove extracellular dextran, only leaving dextran in intracellular vesicles originating from the BL membrane, thus staining NCs in reuptake yellow (red + green). (b) Dextran remained at the BL side during this time period. Data are average ± SEM. *Compares BL vs. AP by Student's t-test ($p<0.05$).**